

# Multi-View Self-Attention for Interpretable Drug-Target Interaction Prediction<sup>☆</sup>

Brighter Agyemang<sup>a,b,\*</sup>, Wei-Ping Wu<sup>a,b</sup>, Michael Yelpengne Kpiebaareh<sup>a,b</sup>,  
Zhihua Lei<sup>a,b</sup>, Ebenezer Nanor<sup>a,b</sup>, Lei Chen<sup>b</sup>

<sup>a</sup>*School of Computer Science and Engineering, University of Electronic Science and Technology of China, Chengdu, P. R. China*

<sup>b</sup>*SipingSoft Co. Ltd., Tianfu Software Park, Chengdu, P. R. China*

---

## Abstract

The drug discovery stage is a vital part of the drug development process and forms part of the initial stages of the development pipeline. In recent times, machine learning-based methods are actively being used to model drug-target interactions for rational drug discovery due to the successful application of these methods in other domains. In machine learning approaches, the numerical representation of molecules is vital to the performance of the model. While significant progress has been made in molecular representation engineering, this has resulted in several descriptors for both targets and compounds. Also, the interpretability of model predictions is a vital feature that could have several pharmacological applications. In this study, we propose a self-attention-based, multi-view representation learning approach for modeling drug-target interactions. We evaluated our approach using three large-scale kinase datasets and compared six variants of our method to 16 baselines. Our experimental results demonstrate the ability of our method to achieve high accuracy and offer biologically plausible interpretations using neural attention.

**Keywords:** Drug-Target Interactions, Machine Learning, Representation Learning, Self-Attention, Drug Discovery

---



---

<sup>☆</sup>This work was supported by SipingSoft Co. Ltd., Chengdu, PRC

<sup>\*</sup>Corresponding author

Email address: [brighteragyemang@gmail.com](mailto:brighteragyemang@gmail.com) (Brighter Agyemang)

## 1. Introduction

In the pharmaceutical sciences, drug discovery is the process of elucidating the roles of compounds in bioactivity for developing novel drugs. The drug discovery stage is a vital part of the drug development process and forms part of the initial stages of the development pipeline. In recent times, traditional *in vivo* and *in vitro* methods for analyzing bioactivities have been enhanced with automated methods such as large-scale High-Throughput Screening (HTS). The automation is motivated by the quest to reduce the cost and time-to-market challenges that are associated with the drug development process. The cost of developing a single drug is estimated to be 1.8 billion US dollars and could take 10-15 years to complete [1]. While HTS provides a better alternative to wet-lab experiments, it is time-consuming (takes about 2-3 years) [2] and requires advanced chemogenomic libraries. Also, with HTS, an exhaustive screening of the known human proteome and the  $10^{60}$  synthetically feasible compounds is intractable [3, 4]. Additionally, HTS has a high failure rate [5].

Lately, the availability of large-scale chemogenomic and pharmacological data (such as DrugBank [6], KEGG [7], STITCH [8], and ChEMBL [9], Davis [10], KIBA [11], PubChem [12]), coupled with advances in computational resources and algorithms have engendered the growth of the *in silico* (computer-based) Virtual Screening (VS) domain. *In silico* methods have the potential to address the challenges mentioned above that plague HTS due to their ability to analyze assay data, unmask inherent relationships, and exploit such latent information for drug discovery tasks [13].

In VS, data-driven models are used to examine and predict Drug-Target Interactions (DTI) to systematically guide subsequent HTS or *in vitro* validation methods. DTI research using VS methods has applications in drug side-effects studies [14] and could be a key contributor in developing personalized medications [15], and in drug-repurposing [16]. Also, it is worth noting that the use of *in silico* methods to optimize the drug development process could reduce healthcare costs and encourage accessibility of healthcare services.

Consequently, there are several *in silico* proposals in the literature about DTI prediction [3]. On account of data usage, structure-based methods, ligand-based approaches, and proteochemometric Modeling (PCM) constitute the taxonomy of existing *in silico* DTI studies. Structure-based methods use the 3D conformations of targets and compounds for bioactivity studies. Docking simulations are well-known instances of structure-based methods. Since the 3D conformations of several targets, such as G-Protein Coupled Receptors (GPCR) and Ion Channels (IC), are unknown, structure-based methods are limited in their application. They are also computationally expensive since a protein could assume multiple conformations depending on its rotatable bonds [3]. Ligand-based methods operate on the assumption that similar compounds would interact with similar targets and vice-versa, tersely referred to as ‘guilt-by-association.’ Hence, ligand-based methods perform poorly when a target has a few known binding ligands ( $< 100$ ). The same applies in reverse.

On the other hand, PCM or chemogenomic methods, proposed in [17], model interactions using a drug (compound)-target (protein) pair as input. Since PCM methods do not suffer from the drawbacks of ligand-based and structure-based methods, there have been many studies in using such chemogenomic methods to study DTIs [18, 19, 20]. Also, PCM methods can use a wide range of drug and target representations. Qiu et al. provide a well-documented growth of the PCM domain [21].

As regards computational methodologies, Chen et al. categorize existing models for DTI prediction into Network-based, Machine Learning (ML)-based, and other models [22]. Network-based methods approach the DTI prediction task using graph-theoretic algorithms where the nodes represent drugs and targets while the edges model the interactions between the nodes [23]. As a corollary, the DTI prediction task becomes a link prediction problem. While network-based methods can work well even on datasets with few samples, they do not generalize to samples out of the training set, among other shortcomings. ML methods tackle the DTI prediction problem by training a parametric or non-parametric model iteratively with a finite independent and identically dis-

tributed training set made up of drug-target pairs using supervised, unsupervised, or semi-supervised algorithms. Probabilistic Matrix Factorization (MF) of an interaction matrix and certain forms of similarity-based methods also exist in the domain [24, 25].

Rifaioğlu et al., in their analysis of recent progress of *in silico* methods, show that researchers in the domain [3] are increasingly studying supervised ML methods. In this context, similarity-based and feature-based methods have been the main ML approaches. Similarity-based methods leverage the drug-drug, target-target, and drug-target similarities to predict new interactions [26, 27, 28]. Feature-based methods represent each drug or target using a numerical vector, which may reflect the entity’s physicochemical and molecular properties. These feature vectors are used to train an ML model to predict unknown interactions. Sachdev et al. provide a thorough discussion of the feature-based DTI methods [29]. Additionally, some proposals combine feature-based and similarity-based methods to model interactions [30, 31]. Due to the recent success of the Deep Learning (DL) domain, a form of ML, in areas such as computer vision [32] and Natural Language Processing (NLP) [33], recent feature-based approaches have mainly been DL algorithms [34, 35, 36, 37, 2, 15].

In feature-based methods, the construction of numerical vectors from the digital forms of drugs or targets is significant. This process is called featurization. The 2D structure of a compound can be represented using a line notation algorithm, such as the Simplified Molecular Input Line Entry System (SMILES) [38]. Likewise, a target can be encoded using amino-acid sequencing. The compound and target features can then be computed using libraries such as RDKit [39] and ProPy [40], respectively. While Wen et al. draw a line between descriptors and fingerprints, we refer to both as descriptors herein since they can be composed to form molecular representations [14].

While significant progress has been made in molecular representation engineering, this has resulted in several descriptors for both targets and compounds [41, 3, 42]. Since the choice of descriptors or features significantly affects model skill, there is an inexorable dilemma for researchers in feature selec-

tion [43, 44]. In some instances, the performance of molecular descriptors tends to be task related [45] and offer complementary behaviors [46, 47, 42]. Therefore, the integration of these predefined descriptors is common and espoused by researchers to construct joint molecular views [48, 3]. Although these descriptors tend to provide domain-related information, their predefined nature means they are unable to establish a closer relationship between the input and output space concerning the task at hand.

Indeed, several algorithms have been proposed to learn compound and target features directly from their sequences, 2D or 3D forms over the past few years [49, 34, 35, 36, 50, 51, 2, 15] using backpropagation. It has been shown that DTI models constructed in such manner usually outperform predefined descriptors or provide competitive results [35, 52, 53]. Nonetheless, the proliferation of these end-to-end descriptor learning methods only exacerbates the dilemma mentioned above since these studies also demonstrate the capabilities of predefined methods such as the Extended Connectivity Fingerprint (ECFP) [54] method.

In another vein, most of the existing DTI studies in the literature have formulated the DTI prediction task as a Binary Classification (BC) problem. However, the nature of bioactivity is continuous. Also, DTI depends on the concentration of the two query molecules and their intermolecular associations [55]. Indeed, it is rare to have a ligand that binds to only one target [3]. While the binary classification approach provides a uniform approach to benchmark DTI proposals in the domain using the GPCR, IC, Enzymes (E), and Nuclear Receptor (NR) datasets of [23], treating DTI prediction as a binding affinity prediction problem leads to the construction of more realistic datasets [56, 11]. Accordingly, the Metz [57], KIBA [11], and Davis [10] datasets serve as the benchmark datasets for regression-based DTI proposals and their output values are measured in dissociation constant ( $K_d$ ), KIBA metric [11], and inhibition constant ( $K_i$ ), respectively. Another significant feature of the regression-based datasets is that they do not introduce class-imbalance problems seen with the BC datasets mentioned above. The BC-based algorithms typically address the class-imbalance

problem using sampling techniques [42] or assume samples without reported interaction information to be non-interacting pairs. We argue that predicting continuous values enable the entire spectrum of interaction to be well-captured in developing DTI prediction models.

Furthermore, since in silico DTI models are typically not replacements for in vitro and in vivo validations, interpretability of their prediction is vital to guiding domain experts to realizing the benefits above of advances in the domain. However, the application of multiple levels of non-linear transformation of the input means that DL models do not lend themselves easily to interpretation. In some studies, less powerful alternatives such as decision trees and  $L_1$  regularization of linear models have been used to achieve the interpretability of prediction results [58, 59]. Recent progress in pooling and attention-based techniques [33, 60, 61] have also aided the ability to gain insights into DL-based prediction results [62, 15]. We posit that such attention-based mechanisms offer a route to provide biologically plausible insights into DL-based DTI prediction models while leveraging the strength of DL-models. Also, since attention-based methods can learn rich molecular representations, it could facilitate accurate predictions in other domains such as ligand-catalyst-target reactions [3].

To this end, our contributions to the domain are as follows:

- We propose a multi-view attention-based architecture for learning the representation of compounds and targets from different unimodal descriptor schemes (including end-to-end schemes) for DTI prediction.
- Our usage of neural attention enables our proposed approach to lend itself to the interpretation and discovery of biologically plausible insights in compound-target interactions across multiple views.
- We also experiment with several baselines and show how these seemingly different compound and target featurization proposals in the literature could be aggregated to leverage their complementary relationships for modeling DTIs.

The rest of our study is organized as follows: section 2 discusses the related work and baseline models of our study, we discuss the various featurization methods we use and our proposed architecture in section 3. The experiments we conducted are described in section 4 and we discuss the results in section 5. Finally, we conclude our work in section 6.

## 2. Related Work

In silico methods provide a promising route to tackle some critical challenges in drug discovery effectively. Over the last decade, several studies have been conducted in modeling interactions, which has led to substantial progress in DTI prediction and other related tasks. We review some of these notable works which relate to our study in what follows.

One of the seminal works on integrating unimodal representations of drugs and compounds is [63]. The authors note that the challenges with DTI prediction mean that the development of models that can leverage heterogeneous data is vital to the domain. Hence, the chemical space, genomic space, and pharmacological space are integrated. Subsequently, the compound-target pairwise relationships are studied using network or graph analysis. Shi et al [26] also augment similarity information with non-structural features to perform DTI prediction using a network-based approach.

Additionally, Luo et al. [64] argue that multi-view representations enable modeling of bioactivities using diverse information. As a result, a DTI model is proposed in [64] that learn the contextual and topological properties of drug, disease, and target networks. Likewise, Wang et al. [65] also propose a random forest-based DTI prediction model that integrates features from drug, disease, target, and side-effect networks learned using GraRep [66]. These network-based DTI models are not scalable to large datasets and unable used on samples outside the dataset.

Also, other researchers have adopted collaborative filtering methods to predict DTIs. In [67], the authors propose a Matrix Factorization (MF) method for

predicting the probability that a compound would interact with a given target. Noting that traditional MF methods are unable to detect nonlinear properties, a deep MF (DMF) method is proposed in [68]. The DMF approach first constructs negative samples using a K-Nearest Neighbor (kNN) method and then builds an interaction matrix. The rows and columns of the interaction matrix then serve as the features of drugs and targets in a DL model, which finds the low-rank decomposition of the interaction matrix.

Similarly, Yasuo et al. [69] use a probabilistic MF approach to decompose an interaction matrix into a target-feature matrix and a feature-ligand matrix. While these DL-based MF are able to learn nonlinear properties, viewing DTI prediction as a BC problem, as seen in these works, does not address the entire spectrum of bioactivity. In [70], the graph-regularized MF approach of [16] is also extended to a multi-view approach that integrates both chemical and structural views of compounds and targets. As mentioned earlier, in the BC setting, true-negatives are mostly lacking and using kNN, as in [68], introduces arbitrariness in determining negative samples.

On the other hand, similarity-based ML methods have also been proposed for DTI prediction. In this setting, compound and target similarity matrices are constructed and used in kernel-based algorithms such as Support Vector Machines (SVM) [71, 72], and other well-known ML algorithms such as kNN and Regularized Least Squares (RLS). While compound similarities are typically constructed by considering their topological and chemical properties [73], target similarities are usually computed using metrics such as the Smith-Watermann (SW) score, which considers the alignment between sequences [74]. Nonetheless, these approaches use the BC problem formulation. Conversely, the work in [55] proposed a Kronecker RLS (KronRLS) method that predicts binding affinity measured in  $K_d$  and  $K_i$ .

Concerning ensemble ML algorithms, SimBoost is proposed in [31] as a GBT-based DTI prediction model. While KronRLS is a linear model, SimBoost can learn non-linear properties for predicting real-valued binding affinities. While [31] uses a feature-engineering step to select compound-target fea-



tures for GBT training, the work in [42] integrates different representations of a target and uses a feature-selection algorithm to construct representations for GBT training. The work in [75] also proposes a feature-selection method for determining feature-subspaces for GBT training. Additionally, [76] proposes an AdaBoost model for DTI prediction. However, as noted in [77], Boosting methods are not well-suited for predicting probabilities.

In another vein, several DL methods have been proposed to learn the features of compounds and targets for DTI prediction [50, 34, 36, 35], whereas others have proposed DL models that take predefined features as inputs. The work in [14] proposed a deep-belief network to model interactions using ECFP and Protein Sequence Composition (PSC) of compounds and targets, respectively. [78] also propose a DTI model that uses generative modeling to oversample the minority class in order to address the class imbalance problem. In [2], the sequence of a target is processed using a Convolutional Neural Network (CNN), whereas a compound is represented using its structural fingerprint. The compound and target feature vectors are concatenated and serve as input to a fully connected DL model. Using CNN means the temporal structure in the target sequence is sacrificed to capture local residue information.

In contrast, [62] used a Recurrent Neural Network (RNN) and Molecular Graph Convolution (MGC) to learn the representations of targets and compounds, respectively. These representations are then processed by a siamese network to predict interactions. A limitation of the approach in [62] is that extending it to multi-task networks require training several siamese models. While all these works formulate the DTI prediction as a BC problem, [56] proposes a DL model that predicts binding affinities given compound and protein encoding. The work in [15] also proposed a self-attention based DL model that predicts binding affinities. Using self-attention enables atom-atom relationships in a molecule to be adequately captured. Nonetheless, these studies do not leverage other unimodal representations of compounds and targets. Also, they do not adopt the split schemes proposed in [55] for developing chemogenomic models.

In what follows, we provide an introduction to the existing regression ML models for DTI prediction that are used as baselines in this study for completeness.

### 2.1. *KronRLS*

The KronRLS method proposed in [55] is a generalization of the RLS method in which the data is assumed to consist of pairs (compounds and targets, in this case). It is a kernel-based approach for predicting the binding affinity between a compound-target pair. Specifically, given a set of compound-target pairs  $X = \{x_1, x_2, \dots, x_m\}$  as training data with their corresponding binding-affinity values  $Y = \{y_1, y_2, \dots, y_m\}$ , where  $i < m$  and  $m \in \mathbb{R}$ , KronRLS learns a real-valued function  $f(x)$  that minimizes the objective,

$$J(f) = \sum_{i=1}^m (y_i - f(x_i))^2 + \lambda \|f\|_k^2 \quad (1)$$

where  $\lambda$  is a regularization parameter and  $\|f\|_k$  is the norm of the minimizer  $f$  associated with the kernel  $k$  in equation 2. Basing on the representer theorem, [55] defines the minimizer as,

$$f(x) = \sum_{i=1}^m a_i k(x, x_i) \quad (2)$$

where the kernel function  $k$  is a symmetric similarity measure between two compound-target pairs. Given a dataset of  $m$  samples,  $k$  can be represented as  $K \in \mathbb{R}^{m \times m}$  computed as  $K_c \otimes K_t$  if  $X$  contains all possible compound-target pairs. Here,  $K_c$  and  $K_t$  are the kernel matrices of the compounds and targets, respectively. In this context, the parameters  $a_i$  of  $f$  can be determined in closed form by solving a system of  $|C||T|$  linear equations:

$$(K + \lambda I)a = y \quad (3)$$

where  $C$  is the set of compounds,  $T$  is the set of targets,  $a \in \mathbb{R}^m$ ,  $y \in \mathbb{R}^m$ , and  $I \in \mathbb{R}^{|C| \times |T|}$  is an identity matrix. Equation 3 assumes that  $Y$  contains the binding affinities of all  $|C| \times |T|$  pairs in order to be solved in closed form. In

cases where this assumption does not hold, conjugate gradient with Kronecker algebraic optimization could be employed to determine  $a$ . However, other imputation strategies have been employed to maintain the closed-form evaluation of equation 3 [55].

## 2.2. SimBoost

SimBoost, proposed in [31], is a gradient boosting approach to predict the binding affinity between a compound and a target. The authors propose three types of features to construct the feature vector of a given compound-target in training set  $X = \{x_1, x_2, \dots, x_m | i < m, m \in \mathbb{R}\}$ :

1. Type 1: features for each compound and target based on average similarity values, and information about their frequency in the dataset.
2. Type 2: features for entities determined from their respective similarity matrices.
3. Type 3: features for each compound-target pair computed using a compound-target network.

Given compound  $c_i$  and target  $t_i$ , the feature vector  $x_i \in \mathbb{R}^d$  of the pair  $c_i - t_i$  is constructed by concatenating the type 1 and type 2 features of both  $c_i$  and  $t_i$ , and the type 3 features of the pair  $c_i - t_i$ . The corresponding binding affinity  $\hat{y}_i$  of  $x_i$  is computed as,

$$\hat{y}_i = \phi(x_i) = \sum_{k=1}^K f_k(x_i), f_k \in \mathbf{F} \quad (4)$$

where  $\mathbf{F}$  is the space of all possible trees and  $K$  is the number of regression trees. Using the additive ensemble training approach, the set of trees  $\{f_k\}$  are learned by minimizing the following regularized objective:

$$L(\phi) = \sum_i l(\hat{y}_i, y_i) + \sum_k \Omega(f_k) \quad (5)$$

where  $\Omega$  determines model complexity to control overfitting,  $l(\cdot)$  is a differentiable loss function which evaluates the prediction error and  $y_i$  is the true binding affinity corresponding to  $x_i$ .

### 2.3. PADME

In [52], PADME is proposed to model DTIs. The authors propose two variants of PADME: PADME-ECFP and PADME-GraphConv. The former variant constructs feature vectors of compounds using the ECFP scheme, whereas the latter learns the representations of compounds using Molecular Graph Convolution [37]. On the other hand, targets are represented using PSC [40]. After that, for a given compound-target pair, the feature vector  $x_i \in \mathbb{R}^d$  is constructed as the concatenation of the compound and target feature vectors. This constructed feature vector then becomes an input to a Fully Connected Neural Network (FCNN) which minimizes the regularized Mean Square Error (MSE) objective,

$$\operatorname{argmin}_{\theta} \sum_{i=0}^N (y_i - f(x_i; \theta))^2 + \lambda \|f\|_k^2 \quad (6)$$

where  $f(x_i; \theta)$  outputs  $\hat{y}_i$  as the predicted value using parameters  $\theta$  and  $\lambda$  is a regularization parameter to control overfitting.

### 2.4. IVPGAN

In our previous study [53], we propose IVPGAN to predict DTIs using a multi-view approach to represent a compound and PSC to construct the target feature vector. While ECFP is used to represent predefined compound features, MGC is used to learn the representation of a compound given the graphical structure encoded in its SMILES notation. Using an Adversarial Loss (AL) training technique, the following objective is minimized:

$$L_G = L_G^{MSE} + \lambda L_G^{AL} \quad (7)$$

where

$$L_G^{MSE} = \sum_{i=0}^N (y_i - f([v_i^c, g(d_i; \theta^g), v_i^p]; \theta^f))^2 + \beta (\|f\|_k^2 + \|g\|_k^2) \quad (8)$$

$$L_G^{AL} = \mathbb{E}_{\mathbf{x} \sim G} [-\log D(\mathbf{x})] \quad (9)$$

,  $\theta^f$  and  $\theta^g$  are trainable parameters,  $g(\cdot) \in \mathbb{R}^d$ ,  $[\dots]$  is a concatenation operator,  $\|\cdot\|_k^2$  is a norm operator,  $\lambda$  is a hyperparameter that is used to control the

combination of MSE and the AL objectives, and  $\beta$  is a regularization parameter that controls overfitting.  $L_G^{MSE}$  is the MSE objective of the DTI prediction model, which is treated as the generator of a Generative Adversarial Network (GAN).  $L_G^{AL}$  is the generator objective component of the GAN whose discriminator objective is expressed as,

$$L_D^{AL} = \mathbb{E}_{\mathbf{x} \sim p} [-\log D(\mathbf{x})] + \mathbb{E}_{\mathbf{x} \sim G} [-\log(1 - D(\mathbf{x}))] \quad (10)$$

where the distributions  $p$  and  $G$  of equations 9 and 10 are derived from the neighborhood alignment matrices constructed from the labels and predicted values, respectively, as explained in [53].

### 3. Methods

#### 3.1. Problem Formulation

We consider the problem of predicting a real-valued binding affinity  $y_i$  between a given compound  $c_i$  and target  $t_i$ ,  $i \in \mathbb{R}$ . The compound  $c_i$  takes the form of a SMILES [38] string, whereas the target  $t_i$  is encoded as an amino acid sequence. The SMILES string of  $c_i$  is an encoding of a chemical graph structure  $d_i = \{V_i, E_i\}$ , where  $V_i$  is the set of atoms constituting  $c_i$  and  $E_i$  is a set of undirected chemical bonds between these atoms. Therefore, each data point in the training set is a tuple  $\langle c_i, t_i, y_i \rangle$ . In this study, we refer to the SMILES of a compound and the amino acid sequence of a target as the ‘raw’ form of these entities, respectively.

In order to use the compounds and targets in VS models, their respective raw forms have to be quantized to reflect their inherent physicochemical properties. Accurately representing such properties is vital to reducing the generalization error of VS models [3]. We discuss the featurization methods considered in our study in sections 3.2 and 3.3.

### 3.2. Compound Featurization

#### 3.2.1. Extended Connectivity Fingerprint

The ECFP algorithm is a state-of-the-art circular fingerprint scheme for numerically encoding the topological features of a compound [54]. ECFP decomposes a compound into substructures and assigns a unique identifier to each fragment. In the algorithm, larger substructures are composed through bond relations. A diameter parameter controls the extent to which these larger substructures can be composed. For instance, with a diameter of 4, (written as ECFP4), the largest substructure has a width of 4 bonds. Subsequently, the unique identifiers of all fragments are hashed to produce a fixed-length binary vector. This final representation indicates the presence of particular substructures. We use RDKit’s [39] implementation of the ECFP algorithm in our study.

#### 3.2.2. Molecular Graph Convolution

Motivated by recent progress in end-to-end representation learning, MGC is a class of algorithms that, for a given layer, apply the same differentiable function to the atoms of a molecule to learn the features of the molecule from its raw form. This operation is akin to the use of kernels in the CNN architecture. Also, information about distant atoms is propagated radially through bonds, as found in circular fingerprints. Thus, composing several layers facilitate the learning of useful representations that are related to the learning objective. The earliest form of MGC is the work in [49]. It has been used in a notable number of studies and in various forms, such as that of [62], to model bioactivity. In [37], graph pool, and gather operations are proposed to augment the neural graph fingerprints algorithm of [49]. Recent progress in the domain has also produced other forms of MGCs [50]. In our study, we use the GraphConv algorithm proposed by [37]. Atom vectors are initialized using predefined physicochemical properties. The main operations of GraphConv are:

1. Graph convolution: applies molecular graph convolution to each atom.
2. Graph pool: applies a pooling function to an atom and its neighbors to get the updated feature vector of the atom.

3. Graph gather: takes the feature vectors of all atoms and applies a down-sampling function to compute the fixed-length compound feature vector

$$x_{molecule} \in \mathbb{R}^d.$$

We refer to the GraphConv implementation without the graph gather operation as GraphConv2D in this study. Hence, for a compound of  $n \in \mathbb{R}$  atoms, where  $a_i \in \mathbb{R}^d, i < n$ , is the vector the  $i$ th atom, the output of GraphConv2D is  $x_{molecule} \in \mathbb{R}^{n \times d}$ .

### 3.2.3. Weave

Weave featurization, proposed in [35], is another form of MGC. In the weave algorithm, atom-atom pairs are constructed using all atoms in a molecule. The features of an atom are then updated using the information of all other atoms and their respective pairs. This form of update enables the propagation of information from distant atoms, albeit with increased complexity. While predefined physicochemical features are used to initialize atom vectors, topological properties are used to initialize atom-atom pair vectors. The following are the main operations of the weave featurization scheme:

1. Weave: applies the weave operation as described above.
2. Weave gather: computes the compound feature vector  $x_{molecule} \in \mathbb{R}^d$  as a function of all atom feature vectors.

We refer to the Weave implementation without the graph gather operation as Weave2D in this study. Thus, for a compound of  $n \in \mathbb{R}$  atoms, where  $a_i \in \mathbb{R}^d, i < n$ , is the vector the  $i$ th atom, the output of Weave2D is  $x_{molecule} \in \mathbb{R}^{n \times d}$ .

### 3.2.4. Graph Neural Network

In [51], a Graph Neural Network (GNN) is proposed for molecular graphs. GNN maps a given molecular graph to a fixed-length feature vector using two differentiable functions: transition and output functions. Atoms are depicted as nodes, and the bonds within a molecule form the edges in the molecular graph. For each entity in the graph, substructures within a specified radius are encoded

to form the embedding profile of the entity. These profiles are then mapped to indices of an embedding matrix that is trained using backpropagation. The transition function is used to update the features of atoms and bonds towards determining the vector representation of the molecule. Thus, applying different transition functions hierarchically recapitulates the convolution operation in a CNN since the same transition function is applied to all entities in the graph in a layer. The output function downsamples the set of node vectors from the transition phase to get the fixed-length molecular representation,  $x_{molecule} \in \mathbb{R}^d$ .

In our study, we use a variant of GNN dubbed GNN2D. This variant omits the downsampling phase of the GNN operation. Thus, for a compound of  $n \in \mathbb{R}$  atoms, where  $a_i \in \mathbb{R}^d, i < n$ , is the vector the  $i$ th atom, the output of GNN2D is  $x_{molecule} \in \mathbb{R}^{n \times d}$ .

### 3.3. Target Featurization

#### 3.3.1. Protein Sequence Composition

As regards target quantization, PSC is a well-known predefined scheme for capturing subsequence information. It consists of Amino Acid Composition (AAC), Dipeptide Composition (DC), and Tripeptide Composition (TC). AAC provides information about the frequency of each amino acid. DC determines the frequency of every two amino acid combinations, whereas TC computes the frequency of every three amino acid combinations. The dimension of a PSC feature vector is 8420.

#### 3.3.2. Prot2Vec

Similar to compound featurization, efforts have been made to learn protein representations directly from their raw forms. Learning protein vectors is typically achieved by learning embedding vectors using NLP techniques such as the word2vec and GloVe models [79, 80]. This approach also maintains the temporal properties in the target sequence. In [81], it is shown that the NLP approach could be used to develop rich target representations. Therefore, we construct a vocabulary of n-gram subsequences (biological words) following the splitting



scheme of [81]. We set  $n = 3$  in this study. In Figure 1, the approach we use to construct the 3-gram profile of a protein sequence is illustrated. The raw form of the protein is split into three non-overlapping representations. The words of all three sequences make up the vocabulary used in this study. We then move across the three splits to construct the overlapping 3-gram target profile. Each word in the dictionary  $D$  is mapped to a randomly initialized vector  $x_i \in \mathbb{R}^d$ ,  $i < |D|$ , that is updated during training.

In order to make computations tractable, we group subsequences using a non-overlapping window approach similar to the method in [51].

Specifically, given the target profile  $\mathcal{S} = \{s_1, s_2, \dots, s_n | n \in \mathbb{R}, n \leq |D|\}$ , we retrieve the vectors of each word to construct the set of vectors  $X = \{x_1, x_2, \dots, x_n\}$ . Setting the window size to 3, for didactic purposes, we group  $X$  as:

$$X = \{[x_1, x_2, x_3], [x_4, x_5, x_6], \dots, [x_{n-2}, x_{n-1}, x_n]\}$$

where  $[\dots]$  is a concatenation operator. Also,  $x_{i:i+w-1}$  denotes the window  $\{x_i, \dots, x_{i+w-1}\}$  where  $w$  is the window size. Note that if  $|x_{i:i+w-1}| < w$  by  $k$  elements, we add  $z \in \mathbb{R}^d$  to the window  $k$  times. Here,  $z$  is a vector of all zeros. Thus, each window is a  $wd$ -dimensional vector. Pooling functions or RNN could then be used to process these windows/segments into a fixed-length representation of the target. In section 3.4 we show how we use our proposed approach to construct the fixed-length vector of a target.

### 3.3.3. Protein Convolutional Neural Network

Protein Convolutional Neural Network (PCNN), proposed by Tsubaki et al. [51], is another end-to-end representation learning scheme for target sequences. It uses a similar approach to the Prot2Vec method (see section 3.3.2), but with overlapping windows, to construct target representations. The subsequent discussion on the PCNN uses Prot2Vec to encode target data and also has a minor variation of the convolution operation in [51]. Given  $c_i^{(l-1)} = x_{i:i+w-1}$  to be the  $i$ th window of  $\mathcal{C}^{(l-1)} = \{c_1^{(l-1)}, c_2^{(l-1)}, \dots, c_{|\mathcal{C}|}^{(l-1)}\}$ , where  $l$  denotes the

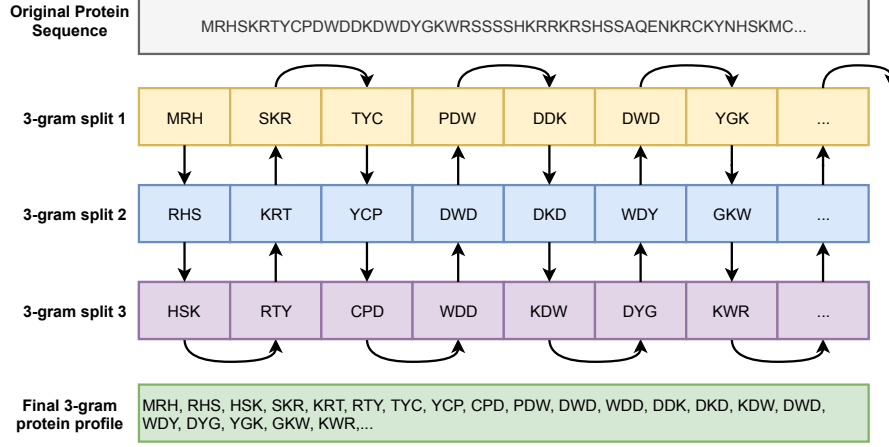


Figure 1: **Target sequence 3-gram representation.** The original target sequence is split into three non-overlapping sequences (split 1, split 2, and split 3). The overlapping 3-gram profile of the protein is constructed by moving across the three sequences as depicted by the arrow.

$l$ th convolution layer, PCNN computes  $c_i^{(l)}$  of  $C^{(l)}$  as,

$$c_i^{(l)} = f(W^l c_i^{(l-1)} + b^{(l)}) \quad (11)$$

where  $f(\cdot)$  is a nonlinear activation function, we let  $W^l \in \mathbb{R}^{wd \times wd}$  be the kernel, and  $b \in \mathbb{R}^{wd}$ . Applying equation 11 multiple times enable nonlinear properties to be learned at different levels of abstraction. In order to produce a  $d$ -dimensional vector  $c_i^{(L)}$  for the last PCNN layer  $L$ , we let  $W^L \in \mathbb{R}^{d \times wd}$  and  $b^L \in \mathbb{R}^d$ . Thus, the final output is  $C^L \in \mathbb{R}^{|C| \times d}$ . We refer to the rows of  $C^L$  as segments.

To compute the vector representation of the target, [51] propose using the average pooling function. It is easy to realize that other differential pooling functions, such as the max and sum functions, could be employed. Moreover, an attention mechanism is proposed in [51], where the compound representation is used to compute attention weights for the segments of the target representation. In this context, the compound vector dimension and the segment dimension must be equal. In this study, we refer to the attention variant as PCNN with Attention (PCNNA). We refer the reader to [51] for the exposition of PCNNA.

Additionally, we use a variant of the PCNN architecture called PCNN2D. This variant omits the downsampling and attention phases of the PCNN method.

### 3.4. Joint View Attention for DTI prediction

We propose a Joint View self-Attention (JoVA) approach to learn rich representations from different unimodal representations of compounds and targets for modeling bioactivity. Such a technique is significant when one considers that there exist several molecular representations, and that other novel methods are likely to be proposed, in the domain.

In Figure 2, we present our proposed DL architecture for predicting binding affinities between compounds and targets. Before discussing the details of the architecture, we explain the terminology it uses:

- Entity: this refers to a compound or target.
- View: this refers to a unimodal representation of an entity.
- Segment: for an entity represented as  $X \in \mathbb{R}^{|X| \times d}$ , we refer to the rows as the segments.
- Projector: projects an entity representation  $X \in \mathbb{R}^{|X| \times d}$  into  $X' \in \mathbb{R}^{|X| \times l}$ , where  $l \in \mathbb{R}$  is the latent space dimension.
- Concatenation function: We denote the concatenation (concat) function as  $[\dots]$ .
- Combined Input Vector (CIV): a vector that is constructed by concatenating two or more vectors and used as the input of a function.

For a set of views  $\mathcal{V} = \{v_1, v_2, \dots, v_J | J \in \mathbb{R}\}$ , JoVA represents  $v_j$  of an entity as  $X_{v_j} \in \mathbb{R}^{|X_{v_j}| \times d_j}$  where  $|X_{v_j}|$  denotes the number of elements that compose the entity and  $d_j \in \mathbb{R}$  is the dimension of the feature vector of each of these elements of the  $j$ -th view. We write  $X_{v_j}$  as  $X_j$  in subsequent discussions to simplify notation. For a compound, the segments are the atoms, whereas a window of  $n$ -gram subsequences is a segment of a target. Note that in the case

where the result of an entity featurization is a vector before applying the JoVA method (e.g., ECFP and PSC), this is seen as  $X_j \in \mathbb{R}^{1 \times d_j}$ . Thus,  $|X_j| = 1$ .

Thereafter, a projection function  $p_j$  of  $v_j$  projects  $X_j$  into a latent space of dimension  $l$  to get  $X'_j \in \mathbb{R}^{|X| \times l}$ . Note that the dimension of each projection function is  $l$ . We refer to this operation as the latent dimension projection. We use the format (seg. denotes segment(s)),

(No. of seg., No. of samples, seg. dimension)

to organize  $N$  samples at this stage, employing zero-padding where necessary due to possible variation in the number of segments in a batch. This data structure follows the usual NLP tensor representation format, where the number of segments is referred to as sequence length. Hence, the output of  $v_j$  for a single entity is written as  $X_j \in \mathbb{R}^{|X| \times 1 \times l}$ . This enables the concatenation of all projected representations to form the joint representation  $[X'_1, X'_2, \dots, X'_J] = \bar{X} \in \mathbb{R}^{K \times 1 \times l}$ , where  $K$  is computed as,

$$K = \sum_{j=1}^J |X_j| \quad (12)$$

$\bar{X}$  then serves as the input to the joint view attention module. Since we use a single data point in our discussion, we use  $\bar{X} \in \mathbb{R}^{K \times l}$  in subsequent discussions.

Figure 3 illustrates the detailed processes between the segment-wise concat and view-wise concat layers of Figure 2. Given the multi-view representation of an entity  $\bar{X}$ , we apply a multihead self-attention mechanism and segment-wise input transformation [61]. An attention mechanism could be thought of as determining the relationships between a query and a set of key-value pairs to compute an output. Here, the query, keys, values, and outputs are vectors. Therefore, given a matrix of queries  $Q$ , a matrix of keys  $K$ , and a matrix of values  $V$ , the output of the attention function is expressed as,

$$Attention(Q, K, V) = softmax\left(\frac{QK^T}{\sqrt{d_k}}\right)V \quad (13)$$

where  $d_k$  is the dimension of  $K$ . In self-attention, we set  $\bar{X}$  as  $Q$ ,  $K$ , and  $V$ . The use of  $\bar{X}$  as query, key, and value enables different unimodal segments to be related to all other views to compute the final representation of the compound-target pair. Thus, each view becomes aware of all other views in learning its representation. This method addresses the challenge of extending the two-way attention mechanism [62] to

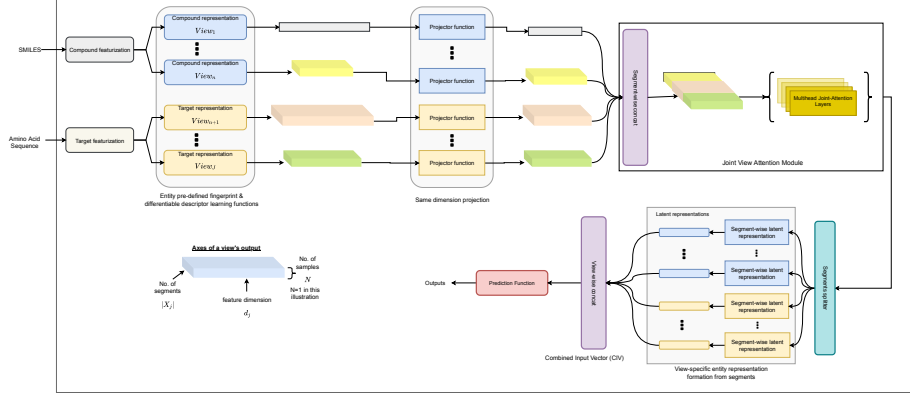


Figure 2: Joint View Attention(JoVA) for Drug-Target Interaction Prediction

multiple unimodal representations. A single computation of equation 13 is referred to as a ‘head’.

In order to learn a rich representation of a compound-target pair,  $\bar{X}$  is linearly projected into different subspaces, and the attention representation of each projection is computed after that. The resulting attention outputs are concatenated and also linear projected to compute the output of the multihead sub-layer. For a set of self-attention heads  $H = \{h_1, h_2, \dots, h_{|H|}\}$ , the multihead function is expressed as,

$$Multihead(Q, K, V) = \text{concat}(H)W^O \quad (14)$$

where  $h_i = \text{Attention}(QW_i^Q, KW_i^K, VW_i^V)$ ,  $W_i^Q \in \mathbb{R}^{l \times d_k}$ ,  $W_i^K \in \mathbb{R}^{l \times d_k}$ ,  $W_i^V \in \mathbb{R}^{l \times d_v}$ ,  $d_v$  is the dimension of  $V$ , and  $W^O \in \mathbb{R}^{|H|d_v \times l}$ .

Additionally, a segment-wise transformation sub-layer is used to transform each segment of the multihead attention sub-layer output non-linearly. Specifically, we compute

$$\hat{X} = \text{ReLU}(a_i W_1 + b_1) W_2 + b_2 \quad (15)$$

where  $a_i$  denotes the  $i$ -th segment,  $W_1 \in \mathbb{R}^{l \times d_{seg}}$ ,  $W_2 \in \mathbb{R}^{d_{seg} \times l}$ . We set  $d_{seg} = 2048$  in this study, same as found in [61].

Furthermore, the Add and Norm layers in Figure 3 implements a residual connection around the multihead and segment-wise transformation sublayers. This is expressed as  $\text{layerNorm}(a_i + \text{sublayer}(a_i))$ .

At the segments splitter layer,  $\hat{X}$  is split into the constituting view representations  $\{\hat{X}_1, \hat{X}_2, \dots, \hat{X}_J\}$ . Note that  $\hat{X}_j \in \mathbb{R}^{X \times l}$  for a single sample. To construct the final

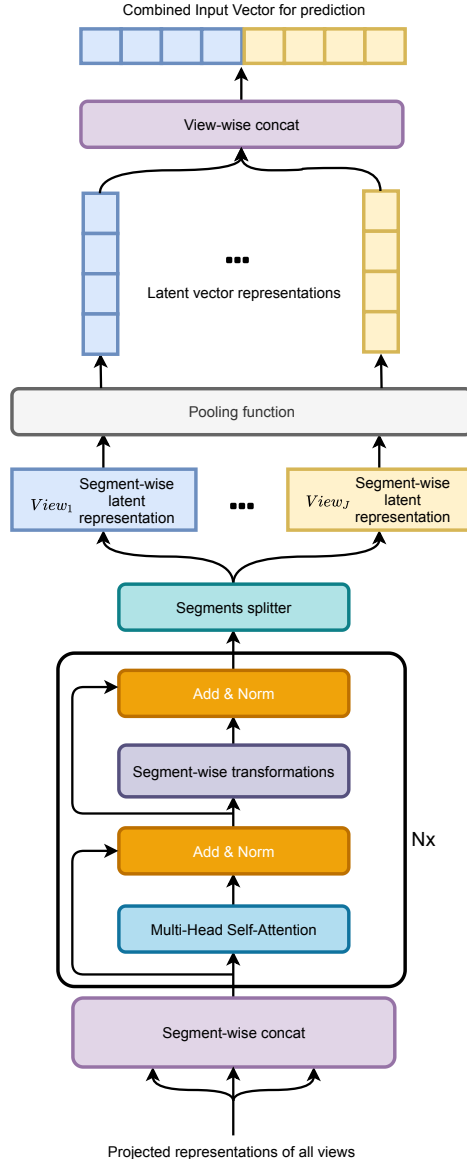


Figure 3: Architecture for constructing of the Combined Input Vector (CIV) using self-attention and pooling given the set of projected unimodal representations.

vector representation  $\nu_j$  out of  $\hat{X}_j$ , pooling functions could then be applied to each view’s representation. This enables our approach to be independent of the number of segments of each view, which could vary among samples. In this study,  $\nu_j \in \mathbb{R}^l$  is computed as,

$$\nu_j = \sum_{i=1}^m \hat{X}_j^{(i)} \quad (16)$$

where  $m = |\hat{X}_j|$  and  $\hat{X}_j^{(i)}$  denotes the  $i$ -th segment of  $\hat{X}_j$ . The view-wise concat layer subsequently computes the final representation of the compound-target pair as the concatenation of  $[\nu_1, \nu_2, \dots, \nu_J]$  to get  $\mathbf{x} \in \mathbb{R}^{Jl}$ . We refer to  $\mathbf{x}$  as the Combined Input Vector (CIV). The CIV therefore becomes the input to a prediction model. In our implementation of JoVA, the prediction model is a FCNN with 2-3 hidden layers.

## 4. Experiments Design

In this section, we present the details of the experiments used to evaluate our proposed approach for DTI prediction.

### 4.1. Datasets

The benchmark datasets used in this study are the Metz [57], KIBA [11], and Davis [10] datasets. These are Kinase datasets that have been applied to benchmark previous DTI studies using the regression problem formulation [55, 73, 31, 52, 15]. Members of the Kinase family of proteins play active roles in cancer, cardiovascular, and other inflammatory diseases. However, their similarity makes it challenging to discriminate within the family. This similarity results in target promiscuity problems for binding ligands and, as a result, presents a challenging prediction task for ML models [55]. We use the version of these datasets curated by [52]. In [52], a filter threshold is applied to each dataset for which compounds and targets with a total number of samples not above the threshold are removed. We maintain these thresholds in our study. The summary of these datasets, after filtering, is presented in table 1. Figure 4 shows the distribution of the binding affinities for the datasets.

### 4.2. Baselines

In line with the multi-view representation learning espoused by this study, we use the following compound and target views listed in Table 3.

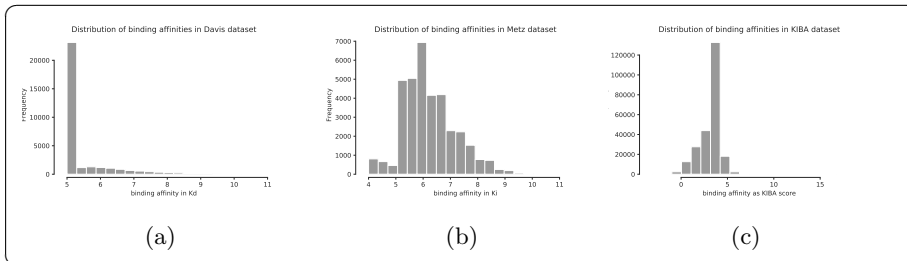


Figure 4: Distribution of the binding affinities (labels) in the Davis, Metz, and KIBA datasets used in our experiments.

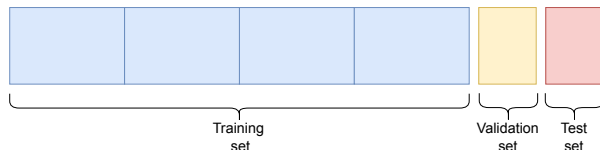


Figure 5: Structure of each fold in the CV scheme used.

We compare our proposed approach to the works in [55, 31, 52, 51]. While [51] is a binary classification model, we replace the endpoint with a regression layer in our experiments. The labels we give to [55, 31] and [51] are KronRLS, SimBoost, and CPI, respectively. SimBoost and KronRLS are implemented as XGBoost and Numpy models, respectively, in our experiments.

As discussed in section 2.3, two DL models were proposed for DTI: (1) PADME-ECFP4 and (2) PADME-GraphConv. Here, we consider these two architectures under a bigger umbrella of models that use a single view of a compound and a single view of a target. The nomenclature of such models is compound view-target view.

In summary, the list of baselines used in this study are presented in Table 4.

#### 4.3. JoVA Models

In order to show the versatility of JoVA, we propose six variants using combinations of the views listed in Table 3. However, other representations not considered herein could be utilized. The primary condition is ensuring that a view’s representation of an entity, before the joint view attention module of Figure 2, is in a matrix form. Indeed, that is the rationale for the 2D variants of the GraphConv, GNN, Weave, and PCNN models. Nonetheless, as earlier mentioned, the feature vector representations could be



Table 1: Dataset sizes

Dataset	Number of compounds /drugs	Number of targets	Total number of pair samples	Filter threshold used
Davis	72	442	31824	6
Metz	1423	170	35259	1
KIBA	3807	408	160296	6

Table 2: Simulation hardware specifications

Model	# Cores	RAM (GB)	Avail. GPUs	# GPUs used
Intel Xeon CPU E5-2687W	48	128	1 GeForce GTX 1080	1
Intel Xeon CPU E5-2687W	24	128	4 GeForce GTX 1080Ti	2

Table 3: Compound and target views used in the experiments

View	Entity	Remark
ECFP8	Compound	See section 3.2.1
GraphConv	Compound	See section 3.2.2
Weave	Compound	See section 3.2.3
GNN	Compound	See section 3.2.4
PSC	Target	See section 3.3.1
RNN	Target	Uses an RNN based on the Prot2Vec target data organization
PCNN	Target	See section 3.3.3

Table 4: Baselines used in experiments

ECFP8-PSC	Weave-PCNNA	GNN-RNN
Weave-PSC	GraphConv-PCNNA	CPI (GNN-PCNNA)
GraphConv-PSC	ECFP8-RNN	SimBoost
GNN-PSC	Weave-RNN	IVPGAN
ECFP8-PCNNA	GraphConv-RNN	IntView (Integrated View)
KronRLS		

Table 5: JoVA variants used in experiments

<b>Compound Views</b>	<b>Target View(s)</b>
ECFP8, GraphConv	PSC
ECFP8, GNN	PSC
ECFP8, GraphConv	PCNN2D
ECFP8, Weave	PSC
ECFP8, GNN	PCNN2D, PSC
ECFP8, GraphConv	RNN, PSC

treated as a one-row matrix in order to make the JoVA computations possible. The six variants are shown in Table 5, and they are implemented as Pytorch models herein.

#### 4.4. Model Training and Evaluation

In our experiments, we used a 5-fold Cross-Validation (CV) model training approach. The structure of each CV-fold is shown in Figure 5. Also, the following three main splitting schemes were used:

- **Warm split:** Every drug or target in the validation and test sets is encountered in the training set.
- **Cold-drug split:** Every compound in the validation and test sets is absent from the training set.
- **Cold-target split:** Every target in the validation and test set is absent from the training set.

Since *cold-start* predictions are typically found in DTI use cases, the cold splits provide realistic and more challenging evaluation schemes for the models.

We used Soek<sup>1</sup>, a Python module based on scikit-learn, to determine the best performing hyperparameters for each of all models. We used the warm split of the Davis dataset and the validation set of each fold for the search. The determined hyperparameters were then kept fixed for all split schemes and datasets. This was done due to the enormous time and resource requirements needed to repeat the search in each case of the experiment. The only exception to this approach is the Simboost model where we searched. In the case of Simboost, we searched for the best performing latent dimension of the matrix factorization stage for each dataset. The test set of each fold was used to evaluate trained models.

As regards evaluation metrics, we measure the Root Mean Squared Error (RMSE) and Pearson correlation coefficient ( $R^2$ ) on the test set in each CV-fold. Additionally, we measure the Concordance Index (CI) on the test set, as proposed by [55].

We follow the averaging CV approach, where the reported metrics are the averages across the different folds. We also repeat the CV evaluation for different random seeds to minimize randomness. After that, all metrics are averaged across the random seeds.

---

<sup>1</sup><https://github.com/bbrighttaer/soek>

## 5. Results and Discussion

In this section, we discuss the results of all baseline and JoVA models of our study. Here, performance is to be understood as referring to the CI, RMSE, and  $R^2$  results of a given model. While the smaller RMSE value is desirable when comparing two models, larger values of CI and  $R^2$  connotes the best performance.

In Figure 6, we present the performances of both the baseline and JoVA models on the Davis dataset. Generally, the cold drug split proved to be the most challenging scheme on the Davis dataset, with the cold target and warm splits following in that order. This trend on the Davis dataset implies that the entity with fewer samples may offer the toughest challenge in the cold splitting schemes of [55].

We realized that the models that utilized multiple unimodal representations of entities usually resulted in the best or competitive performance on the RMSE, CI, and  $R^2$  metrics. In particular, the IntView and IVPGAN models performed best amongst all the models, with the IntView model attaining a marginal increase in performance than the IVPGAN model. While the IVPGAN results observed in this study is an improvement on the work in [53]. Nonetheless, the ECFP8-PSC model performed almost as well as the best performing multi-view methods. We argue that the simplicity (in terms of the number of trainable parameters) of the ECFP8-PSC model makes it suitable to perform well on the Davis dataset. Thus, we reckon that the susceptibility of the CPI, ECFP8-PCNNA, GNN-RNN, GraphConv-PCNNA/RNN, and Weave-RNN models to overfitting accounts for their respective gap in performance, given the size of the Davis dataset.

Also, while the CPI (GNN-PCNNA) model performed poorly, the GNN-PSC model attained competitive performance, especially on the warm and cold target splits. Thus, we show that the GNN method proposed in [51] could be paired with other target representations, other than PCNNA, to improve performance. Interestingly, the richness of the PSC representation is seen in the inability of the PCNNA and RNN baseline models to perform well on the Davis dataset. An instance of this phenomenon is seen in the Weave-PSC, and Weave-RNN reported results. While this presents a counter-intuitive observation, we posit that on more massive datasets, such end-to-end target representation methods could, at the minimum, produce comparative results to models that use predefined features.

As regards the traditional ML models, KronRLS recorded modest results for a

linear model, whereas SimBoost achieved results comparable to that of the multi-view baseline models. While the performance of GBT is well documented in the literature, we note that our approach to determining the MF latent dimension also contributes to the improvement in the results since [31] shows the significance of the MF features to model predictions.

On the other hand, the ECFP8-GraphConv-RNN-PSC and ECFP8-GNN-PSC models demonstrate the effectiveness of the proposed attention-based approach for integrating multiple unimodal representations of entities for DTI. Similar to the DL baseline models, more complex JoVA models performed somewhat poorly, albeit less so in juxtaposition with their baseline analogs. We argue that this is due to the attention mechanism’s ability to actively encourage learning representations that are highly related to the learning objective. While the IVPGAN and IntView models attained the best performance on the Davis dataset, the best performing JoVA models offer the ability to interpret prediction results via examining the attention weights, aside from the high prediction performance. Additionally, the reported results of the best JoVA models seem to imply that the attention-based multi-view representation learning approach reduces the challenge of the cold splitting schemes. For instance, comparing the results of the GNN-PSC and ECFP8-GNN-PSC models emphasizes the ability of JoVA on the cold target scheme. Thus, our proposed method of modeling bioactivity attains respectable results on the Davis benchmark dataset.

The performance of the baseline and JoVA models on the Metz datasets are shown in Figure 7. Similar to the general trend of difficulty seen on the Davis dataset, the cold target regime proved to be the most challenging since the Metz dataset set has fewer targets (see Table 1). This phenomenon is more evident among the baseline models than the JoVA models.

Furthermore, the DL-based baselines mostly performed poorly on the Metz dataset. In particular, the GraphConv-RNN/PCNNA and CPI models attained performances similar to the KronRLS model. This observation connotes that massive bioactivity datasets are required in the domain for training unimodal end-to-end DTI models in order to learn abstract nonlinear patterns from samples properly. It is noteworthy that while SimBoost edged the multi-view models to become the best performing model, the nature of SimBoost’s feature engineering phase renders it inapplicable to the cold splitting schemes. Additionally, while all other baselines and JoVA models maintain

the hyperparameters identified using the warm splitting scheme of the Davis dataset, the MF phase of SimBoost uses hyperparameters explicitly identified for the Metz dataset.

We also observe from Figure 7b that the results of the JoVA models on the Metz dataset consistently follow their respective results on the Davis dataset. We argue that this behavior is a direct result of the attention-based multi-view representation learning approach proposed in this study. Here, the ECFP8-GNN-PSC, ECFP8-GraphConv-PSC, and ECFP8-GraphConv-RNN-PSC models recorded the best results. An interesting highlight is how the JoVA models’ performances are almost invariable in all three splitting schemes as compared to the variations seen among the baselines. For instance, comparing the ECFP8-GNN-PSC JoVA model to the GNN-PSC, ECFP8-PSC, IVPGAN baselines reify this phenomenon.

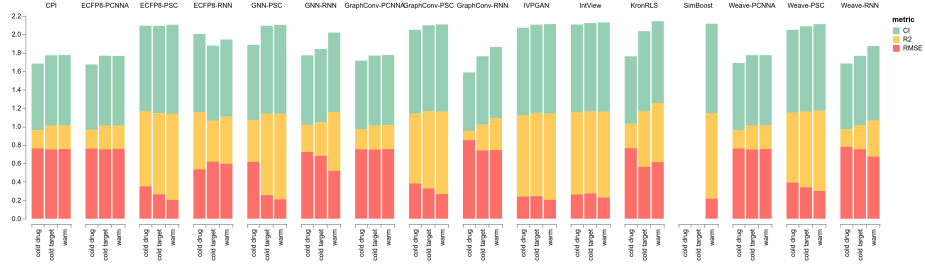
Likewise, comparing the CPI (GNN-PCNNA) baseline to the ECFP8-GNN-PCNN2D-PSC JoVA model gives another perspective into the strengths of our proposed approach. ECFP8-GNN-PCNN2D-PSC, as could be deduced from our earlier discussions, uses the GNN and PCNN modules of the CPI architecture. However, while CPI performs poorly on the Metz dataset, the joint view attention mechanism leverages ECFP8 and PSC to cause better results in the ECFP8-GNN-PCNN2D-PSC model.

On the KIBA dataset, while most of the baselines had varied in their performances (see Figure 8), the JoVA models performed similarly to the previous experiments. This demonstrates the consistency of our approach across different datasets. In particular, it can be seen that the ECFP8-GraphConv-RNN-PSC performed just as well as recorded on the Metz and Davis datasets. Additionally, in Figures 9-11 also present the plots of the ECFP8-GraphConv-RNN-PSC model on the three datasets used in this study. The foregoing performance consistency claim on all three CV splits also agrees with the scatter and joint plots shown in these figures.

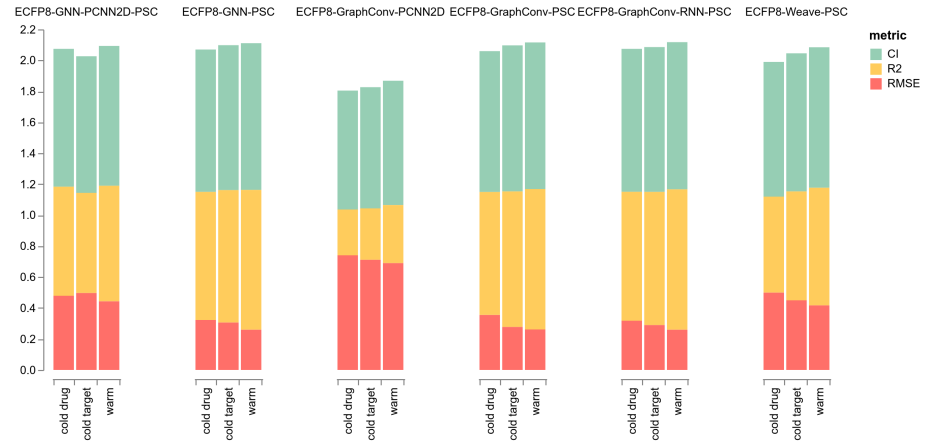
Taken together, we believe that using self-attention to align multiple unimodal representations of atoms and amino acid residues to each other enables a better representational capacity, as is typical of most neural attention-based DL models.

### 5.1. DrugBank Case Study

In this section, we discuss a case study performed using the Drugbank [82] database. The ECFP8-GraphConv-RNN-PSC model trained on the KIBA dataset using the

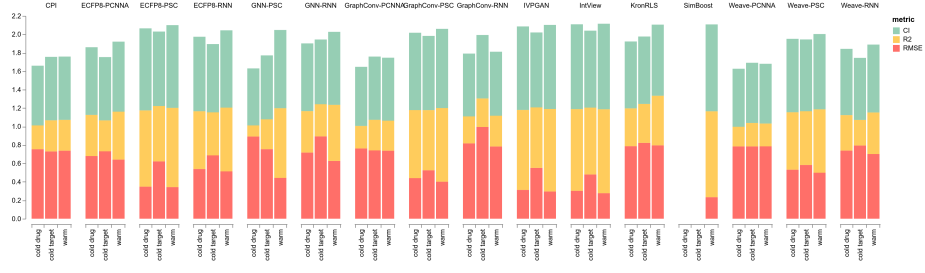


(a)

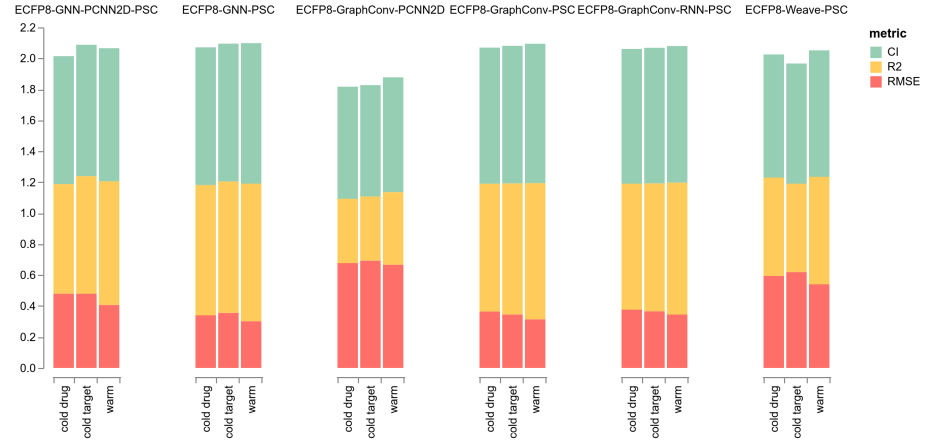


(b)

Figure 6: **Davis dataset results.** (a) Performance of baseline models. (b) Performance of JoVA models.



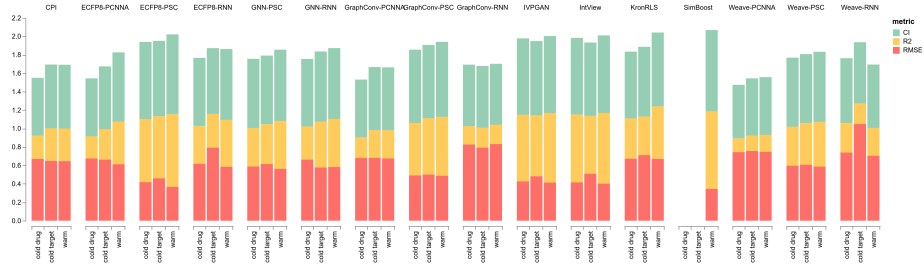
(a)



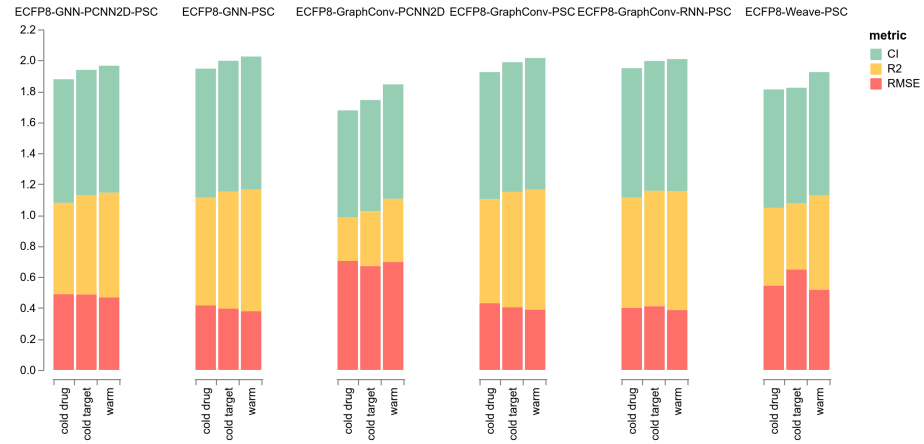
(b)

Figure 7: **Metz dataset results.** (a) Performance of baseline models. (b) Performance of JoVA models.





(a)



(b)

Figure 8: **KIBA dataset results.** (a) Performance of baseline models. (b) Performance of JoVA models.

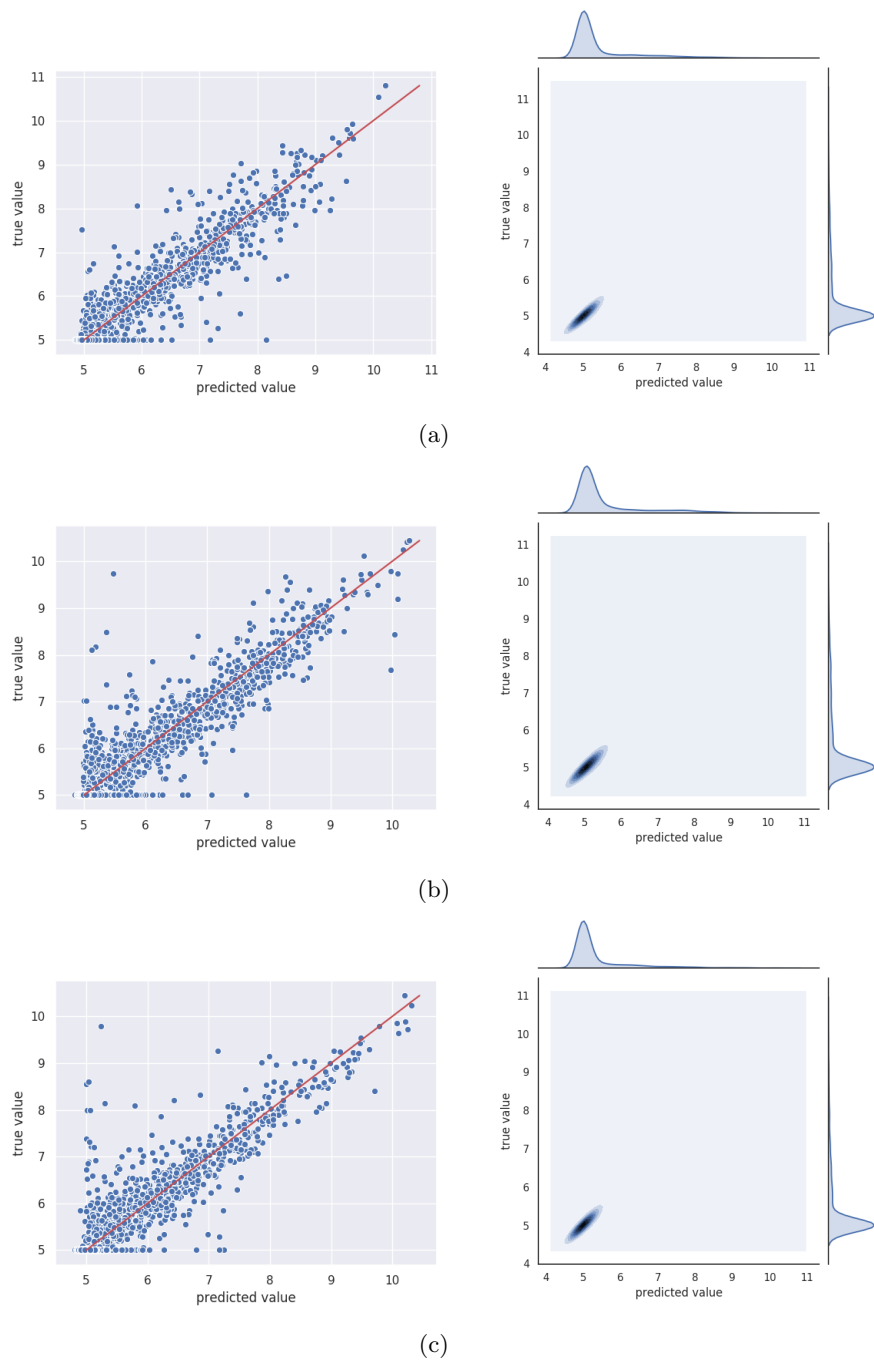


Figure 9: **ECFP8-GraphConv-RNN-PSC results on the Davis dataset.** (From right to left) Column 1 shows the scatter plots of the ground truth (red line) against predicted values (blue dots). Column 2 shows the joint distribution plots of the ground truth against predicted values. The first, second, and third rows correspond to the warm, cold drug, and cold target splits, respectively.

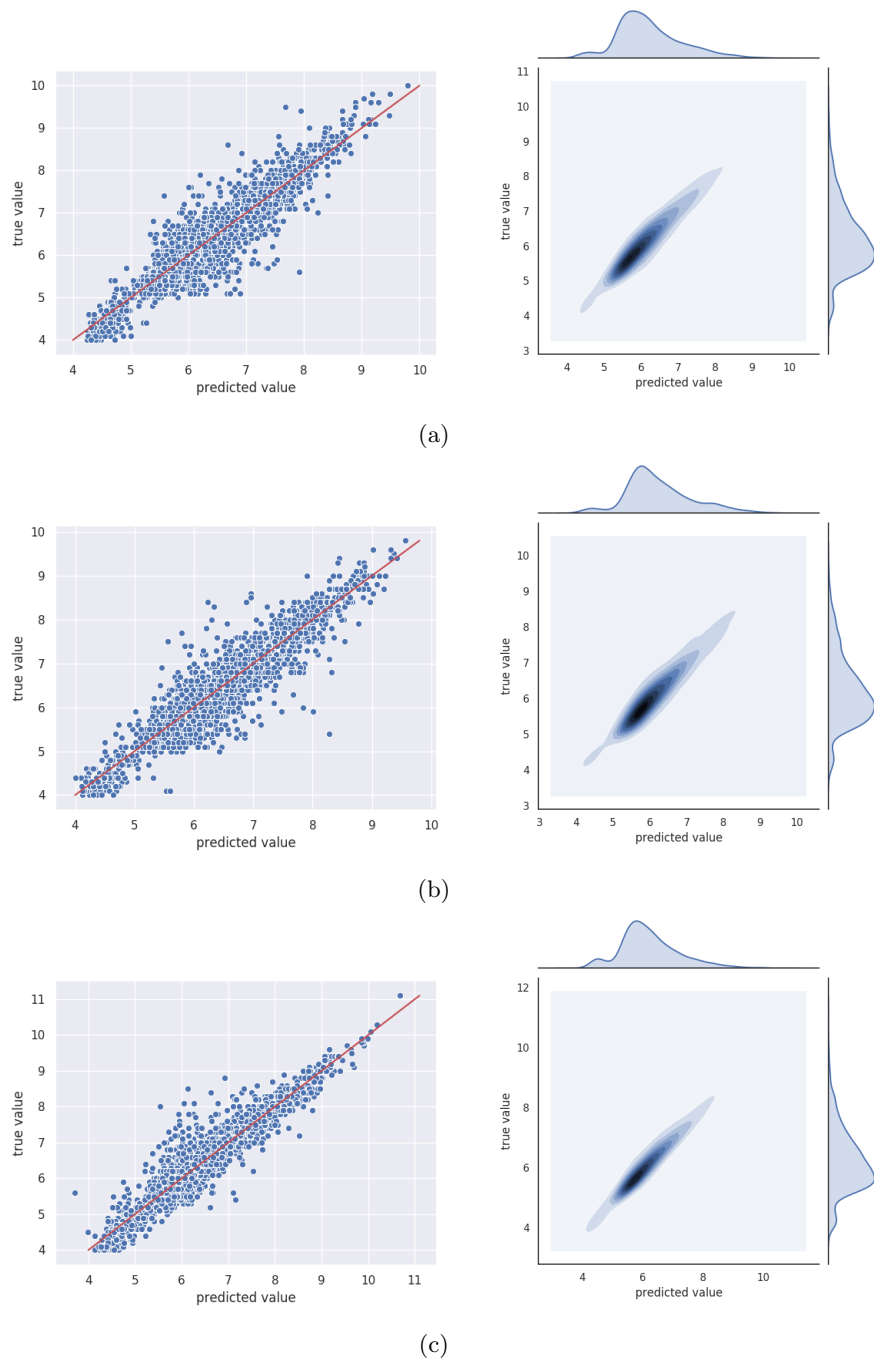


Figure 10: **ECFP8-GraphConv-RNN-PSC results on the Metz dataset.** (From right to left) Column 1 shows the scatter plots of the ground truth (red line) against predicted values (blue dots). Column 2 shows the joint distribution plots of the ground truth against predicted values. The first, second, and third rows correspond to the warm, cold drug, and cold target splits, respectively.

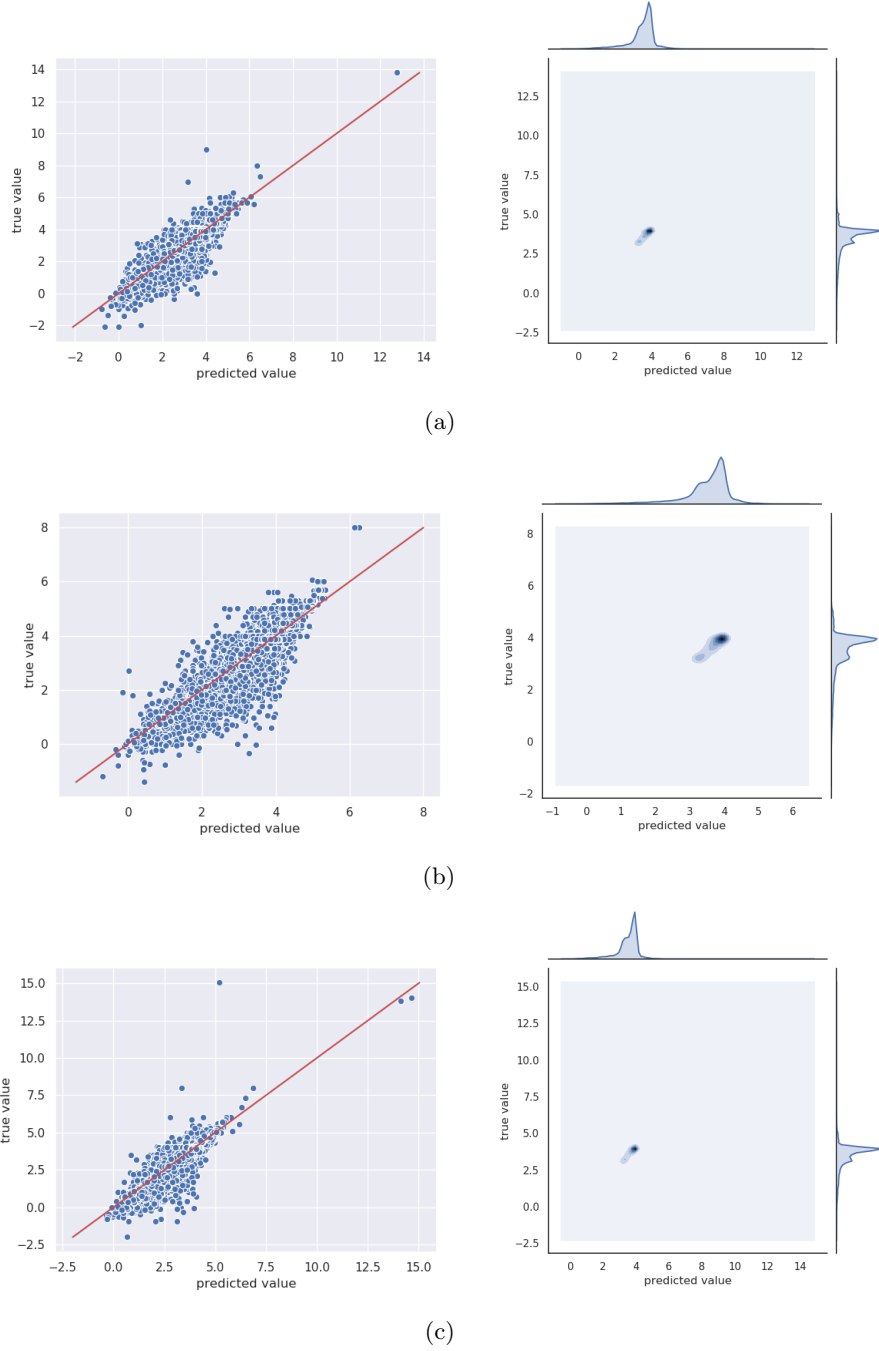


Figure 11: **ECFP8-GraphConv-RNN-PSC results on the KIBA dataset.** (From right to left) Column 1 shows the scatter plots of the ground truth (red line) against predicted values (blue dots). Column 2 shows the joint distribution plots of the ground truth against predicted values. The first, second, and third rows correspond to the warm, cold drug, and cold target splits, respectively.

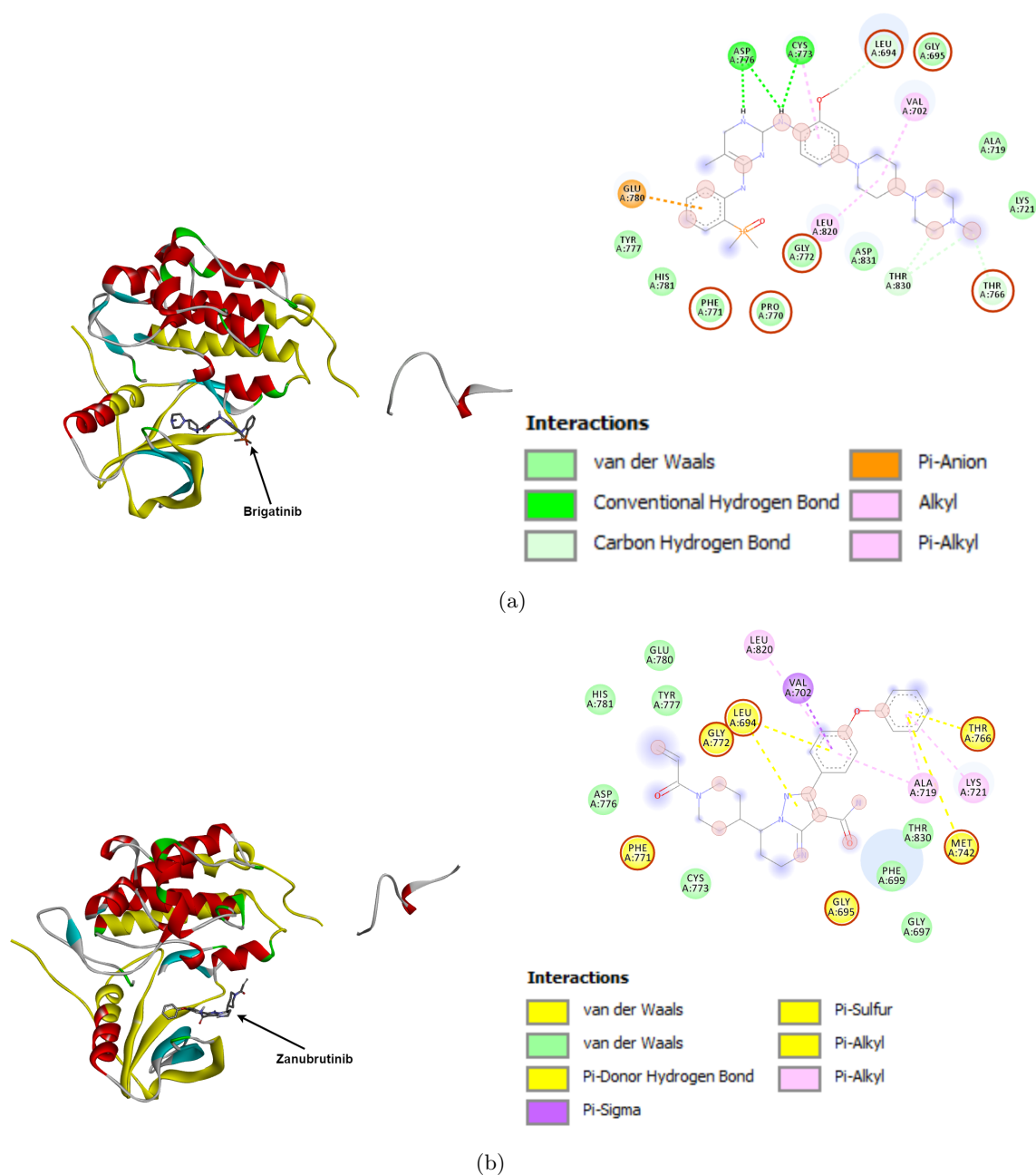


Figure 12: Epidermal Growth Factor Receptor (EGFR-1M17) tyrosine kinase domain in complex with (a) Brigatinib and (b) Zanubrutinib. The amino acid residues in yellow represent the top-10 subsequences predicted by the JoVA model. For both complexes, the corresponding interaction analysis of the ligand in the binding pocket of EGFR-1M17 is shown on the right. The top-10 atoms of ligand predicted by the JoVA model to be influential in the interaction are depicted in transparent red circles. The amino acids shown in the interaction analysis and also among the top-10 residues in each complex are highlighted using red circles as borders.

warm split scheme was selected to evaluate the ability of our approach to predict novel and existing interactions.

The human Epidermal Growth Factor Receptor (EGFR) was selected to be the target for the case study. While other targets could equally be chosen, EGFR was selected since it is implicated in breast cancer and is a popular target for cancer therapeutics. As regards this Drugbank case study, we refer to both the approved and investigational drug relations of EGFR as interactions.

We downloaded 13,339 compounds from the Drugbank database containing 30 interaction records for EGFR. Since the Drugbank database contains small and biological molecules, we filtered out all biologics. The filtered dataset contained 10,630 small molecules, of which 21 are reported to target EGFR. Also, we removed all compounds that are present in the KIBA dataset to ensure that all drugs used for the case study were not part of the training set. As a result, the size of the final Drugbank dataset used for this case study was 9,484, with 8 EGFR interactions. Thus, 13 of the 21 small molecules in the Drugbank database are also present in the KIBA dataset.

In table 6 we present the top-50 predictions of the JoVA model. The model was able to have 6 of the 8 EGFR interactions in its first 50 drugs, ranked according to the KIBA score. Also, it can be seen that the predicted KIBA scores for all the reported drugs fall under the  $KIBA \leq 3.0$  threshold used in [28] to indicate true interactions. Using the unfiltered 10,630 small molecules, the predicted KIBA values of 17 of the 21 EGFR interactions were all below the threshold mentioned above, with the remaining 4 falling under 4.0.

While these results demonstrate the ability of our proposed approach to improve the virtual screening stage of drug discovery, the novel predictions reported herein could become possible cancer therapeutics upon further investigations.

## 5.2. Interpretability Case Study

As mentioned earlier, the interpretability of DTI predictions could facilitate the drug discovery process. Also, being able to interpret an interaction in both the compound and target directions of the complex could reveal abstract intermolecular relationships.

Therefore, we performed an interpretability case study using Brigatinib and Zanubrutinib as the ligands and EGFR (Protein Data Bank ID: 1M17) as the macromolecule

Table 6: The top 50 drugs predicted to interact with the Epidermal Growth Factor Receptor by the ECFP8-GraphConv-RNN-PSC JoVA model. Entries in **bold print** are drugs reported to target EGFR in the Drugbank database. The chemical formula of a drug is used if the name of the drug is long.

Rank	Drugbank ID	Drug	KIBA score
1	DB11963	<b>Dacomitinib</b>	1.314
2	DB06021	<b>AV-412</b>	1.516
3	DB07788	$C_{19}H_{22}O_7$	1.693
4	DB12818	NM-3	1.775
5	DB14944	Tarloxotinib	1.834
6	DB02848	$C_{22}H_{22}N_4O_3S$	1.901
7	DB05944	<b>Varlitinib</b>	1.912
8	DB12669	4SC-203	1.915
9	DB12114	Poziotinib	1.993
10	DB14993	Pyrotinib	1.997
11	DB06346	Fiboflapon	2.172
12	DB11652	Tucatinib	2.301
13	DB01933	7-Hydroxystaurosporine	2.414
14	DB12381	Merestinib	2.423
15	DB07270	$C_{20}H_{15}Cl_2N_3O_4S$	2.467
16	DB06469	Lestaurtinib	2.534
17	DB13517	Angiotensinamide	2.582
18	DB09027	Ledipasvir	2.591
19	DB11747	Barasertib	2.645
20	DB12668	Metenkefalin	2.654
21	DB03482	$C_{28}H_{36}N_{10}O_{15}P_2$	2.692
22	DB11613	Velpatasvir	2.693
23	DB07321	$C_{20}H_{15}Cl_2N_3O_5S$	2.706
24	DB03005	$C_{42}H_{45}N_8$	2.708
25	DB13088	AZD-0424	2.708
26	DB12673	ATX-914	2.712
27	DB12267	<b>Brigatinib</b>	2.717
28	DB11973	Tesevatinib	2.721
29	DB12706	Seletalisib	2.724
30	DB15343	HM-43239	2.755
31	DB12183	Sapitinib	2.764
32	DB15035	<b>Zanubrutinib</b>	2.764
33	DB15168	Cilofexor	2.772
34	DB06915	$C_{10}H_8O_5$	2.777
35	DB11853	Relugolix	2.778
36	DB15407	Acalisib	2.797
37	DB05038	Anatibant	2.821
38	DB14795	AZD-3759	2.837
39	DB06638	Quarfloxin	2.837
40	DB01763	$C_{21}H_{28}N_7O_{16}P_3S$	2.857
41	DB15403	Ziritaxestat	2.859
42	DB12557	FK-614	2.859
43	DB07838	$C_{17}H_{12}N_2O_4S_2$	2.864
44	DB11764	Spebrutinib	2.866
45	DB07698	$C_{18}H_{14}ClN_5$	2.869
46	DB13164	<b>Olmutinib</b>	2.879
47	DB12064	BMS-777607	2.912
48	DB09183	Dasabuvir	2.914
49	DB06666	Lixivaptan	2.934
50	DB06734	Bafilomycin B1	2.937

in two case studies. The EGFR structure was retrieved from the PDB<sup>2</sup> and the ligand structures from the DrugBank for docking experiments. We used PyRx [83] to perform in-silico docking and Discovery Studio (v20.1.0) to analyze the docking results. We then mapped the top-10 atoms and top-10 amino acid residues predicted by the JoVA model used in the Drugbank case study above unto the docking results. The attention outputs of the model were used in selecting these top-k segments. In Figure 12, the yellow sections of the macromolecule indicate the top-10 amino acid residues, whereas the top-10 atoms of the ligand are shown in red transparent circles in the interaction analysis results on the right of each complex.

In the case of the EGFR-Brigatinib complex (see Figure 12a), we realized that the selected amino acid residues were mostly around the binding pocket of the complex. While we show only the best pose of the ligand in Figure 12, the other selected amino acid residues were identified by the docking results to be for other poses of the ligand. Also, selected atoms of the ligand happen to be either involved in an intermolecular bond or around regions identified by the docking results analysis to be essential for the interaction. Interestingly, the amino acids of the macromolecule identified to be intimately involved in the interaction and also among the top-10 residues are predominantly in a Vand der Waals interaction with the ligand. Thus, the model considered stability of the interaction at the active site to be significant in determining the binding affinity.

Likewise, the EGFR-Zanubrutinib case study yielded interpretable results upon examination. It could be seen in Figure 12b that the top-10 amino acid residues selected in the EGFR-Brigatinib case study were identified again. Thus, the model has learned to consistently detect the binding site in both case studies. Indeed, this consistency was also observed in several other experiments using EGFR-1M17 and other ligands<sup>3</sup>. This aligns with knowledge in the domain where an active site could be targeted by multiple ligands. The highlighted top-10 amino acid residues also contain three phosphorylation sites (Thr686, Tyr740, Ser744), according to the NetPhos 3.1 [84]<sup>4</sup> server prediction results. Additionally, the interaction analysis of the EGFR-Zanubrutinib case study reveals that a number of the amino acids selected in the top-10 segments

---

<sup>2</sup><https://www.rcsb.org/structure/1M17>

<sup>3</sup>The CSV file containing all the results could be retrieved at <https://shorturl.at/guKQZ>

<sup>4</sup><https://services.healthtech.dtu.dk/>



are involved in pi-interactions which are vital to protein-ligand recognition. We also note that some of the selected atoms of Zanubrutinib are in the aromatic regions where these pi-interactions take place. In another vein, other selected amino acids are involved in Vand der Waals interactions which reinforce the notion of stability being significant in determining the binding affinity.

In the nutshell, our approach is also able to offer biologically plausible cues to experts for understanding DTI interactions. Such an ability could be invaluable in improving existing virtual screening methods in rational drug discovery.

## 6. Conclusion

In this study, we have discussed the significance of studying DTI as a regression problem and also highlighted the advantages that lie within leveraging multiple entity representations for DTI prediction. Our experimental results indicate the effectiveness of our proposed self-attention based method in predicting binding affinities and offers biologically plausible interpretations via the examination of the attention outputs. The ability to learn rich representations using the self-attention method could have applications in other cheminformatic and bioinformatic domains such as drug-drug and protein-protein studies.

## Acknowledgement

We would like to thank Siqing Zhang and Chenquan Huang for their help in setting up the experiment platforms. We are also grateful to Orlando Ding, Obed Tettey Nartey, Daniel Addo, and Sandro Amofa for their insightful comments. We thank all reviewers of this study.

## References

- [1] A. L. Hopkins, Drug discovery: Predicting promiscuity (2009). doi:10.1038/462167a.
- [2] I. Lee, J. Keum, H. Nam, DeepConv-DTI: Prediction of drug-target interactions via deep learning with convolution on protein sequences, PLoS Computational Biology 15 (6) (2019) 1–21. arXiv:1811.02114, doi:10.1371/journal.pcbi.1007129.

- [3] A. S. Rifaioğlu, H. Atas, M. J. Martin, R. Cetin-Atalay, V. Atalay, T. Doan, Recent applications of deep learning and machine intelligence on in silico drug discovery: methods, tools and databases, *Briefings in Bioinformatics* (January) (2018) 1–36. doi:10.1093/bib/bby061.  
URL <https://academic.oup.com/bib/advance-article/doi/10.1093/bib/bby061/5062947>
- [4] P. G. Polishchuk, T. I. Madzhidov, A. Varnek, Estimation of the size of drug-like chemical space based on GDB-17 data, *Journal of Computer-Aided Molecular Design* doi:10.1007/s10822-013-9672-4.
- [5] T. N. Doman, S. L. McGovern, B. J. Witherbee, T. P. Kasten, R. Kurumbail, W. C. Stallings, D. T. Connolly, B. K. Shoichet, Molecular docking and high-throughput screening for novel inhibitors of protein tyrosine phosphatase-1B, *Journal of Medicinal Chemistry* doi:10.1021/jm010548w.
- [6] C. Knox, V. Law, T. Jewison, P. Liu, S. Ly, A. Frolkis, A. Pon, K. Banco, C. Mak, V. Neveu, Y. Djoumbou, R. Eisner, A. C. Guo, D. S. Wishart, Drug-Bank 3.0: A comprehensive resource for 'Omics' research on drugs, *Nucleic Acids Research* doi:10.1093/nar/gkq1126.
- [7] M. Kanehisa, S. Goto, Y. Sato, M. Furumichi, M. Tanabe, KEGG for integration and interpretation of large-scale molecular data sets, *Nucleic Acids Research* doi:10.1093/nar/gkr988.
- [8] D. Szklarczyk, A. Santos, C. Von Mering, L. J. Jensen, P. Bork, M. Kuhn, STITCH 5: Augmenting protein-chemical interaction networks with tissue and affinity data, *Nucleic Acids Research* doi:10.1093/nar/gkv1277.
- [9] A. P. Bento, A. Gaulton, A. Hersey, L. J. Bellis, J. Chambers, M. Davies, F. A. Krüger, Y. Light, L. Mak, S. McGlinchey, M. Nowotka, G. Papadatos, R. Santos, J. P. Overington, The ChEMBL bioactivity database: An update, *Nucleic Acids Research* doi:10.1093/nar/gkt1031.
- [10] M. I. Davis, J. P. Hunt, S. Herrgard, P. Ciceri, L. M. Wodicka, G. Pallares, M. Hocker, D. K. Treiber, P. P. Zarrinkar, Comprehensive analysis of kinase inhibitor selectivity., *Nature biotechnology* doi:10.1038/nbt.1990.

- [11] J. Tang, A. Sz wajda, S. Shakyawar, T. Xu, P. Hintsanen, K. Wennerberg, T. Aitokallio, Making sense of large-scale kinase inhibitor bioactivity data sets: A comparative and integrative analysis, *Journal of Chemical Information and Modeling* doi:10.1021/ci400709d.
- [12] S. Kim, P. A. Thiessen, E. E. Bolton, J. Chen, G. Fu, A. Gindulyte, L. Han, J. He, S. He, B. A. Shoemaker, J. Wang, B. Yu, J. Zhang, S. H. Bryant, PubChem substance and compound databases, *Nucleic Acids Research* doi:10.1093/nar/gkv951.
- [13] A. C. Schierz, Virtual screening of bioassay data, *Journal of Cheminformatics* doi:10.1186/1758-2946-1-21.
- [14] M. Wen, Z. Zhang, S. Niu, H. Sha, R. Yang, Y. Yun, H. Lu, Deep-Learning-Based Drug-Target Interaction Prediction, *Journal of Proteome Research* doi:10.1021/acs.jproteome.6b00618.
- [15] B. Shin, S. Park, K. Kang, J. C. Ho, Self-Attention Based Molecule Representation for Predicting Drug-Target Interaction (2019) 1–18 arXiv:1908.06760.  
URL <http://arxiv.org/abs/1908.06760>
- [16] A. Ezzat, P. Zhao, M. Wu, X. L. Li, C. K. Kwok, Drug-target interaction prediction with graph regularized matrix factorization, *IEEE/ACM Transactions on Computational Biology and Bioinformatics* 14 (3) (2017) 646–656. doi:10.1109/TCBB.2016.2530062.
- [17] M. Lapinsh, P. Prusis, A. Gutcaits, T. Lundstedt, J. E. Wikberg, Development of proteo-chemometrics: a novel technology for the analysis of drug-receptor interactions, *Biochimica et Biophysica Acta (BBA) - General Subjects* 1525 (1) (2001) 180 – 190. doi:[https://doi.org/10.1016/S0304-4165\(00\)00187-2](https://doi.org/10.1016/S0304-4165(00)00187-2).  
URL <http://www.sciencedirect.com/science/article/pii/S0304416500001872>
- [18] M. Lapinsh, P. Prusis, S. Uhln, J. E. S. Wikberg, Improved approach for proteochemometrics modeling: application to organic compoundamine G protein-coupled receptor interactions, *Bioinformatics* 21 (23) (2005) 4289–4296. arXiv:<https://academic.oup.com/bioinformatics/article-pdf/21/>

23/4289/6139389/bti703.pdf, doi:10.1093/bioinformatics/bti703.

URL <https://doi.org/10.1093/bioinformatics/bti703>

- [19] I. Corts-Ciriano, Q. U. Ain, V. Subramanian, E. B. Lenselink, O. Mndez-Lucio, A. P. IJzerman, G. Wohlfahrt, P. Prusis, T. E. Malliavin, G. J. P. van Westen, A. Bender, Polypharmacology modelling using proteochemometrics (pcm): recent methodological developments, applications to target families, and future prospects, *Med. Chem. Commun.* 6 (2015) 24–50. doi:10.1039/C4MD00216D. URL <http://dx.doi.org/10.1039/C4MD00216D>
- [20] P. Manoharan, K. Chennou, N. Ghoshal, Target specific proteochemometric model development for bace1 protein flexibility and structural water are critical in virtual screening, *Mol. BioSyst.* 11 (2015) 1955–1972. doi:10.1039/C5MB00088B. URL <http://dx.doi.org/10.1039/C5MB00088B>
- [21] T. Qiu, J. Qiu, J. Feng, D. Wu, Y. Yang, K. Tang, Z. Cao, R. Zhu, The recent progress in proteochemometric modelling: Focusing on target descriptors, cross-term descriptors and application scope, *Briefings in Bioinformatics*doi:10.1093/bib/bbw004.
- [22] X. Chen, C. C. Yan, X. Zhang, X. Zhang, F. Dai, J. Yin, Y. Zhang, Drug-target interaction prediction: Databases, web servers and computational models, *Briefings in Bioinformatics* 17 (4) (2016) 696–712. doi:10.1093/bib/bbv066.
- [23] Y. Yamanishi, M. Araki, A. Gutteridge, W. Honda, M. Kanehisa, Prediction of drug-target interaction networks from the integration of chemical and genomic spaces, *Bioinformatics*doi:10.1093/bioinformatics/btn162.
- [24] M. C. Cobanoglu, C. Liu, F. Hu, Z. N. Oltvai, I. Bahar, Predicting drug-target interactions using probabilistic matrix factorization, *Journal of Chemical Information and Modeling*doi:10.1021/ci400219z.
- [25] L. Chen, W.-M. Zeng, A Two-step Similarity-based Method for Prediction of Drug’s Target Group, *Protein & Peptide Letters*doi:10.2174/0929866511320030015.
- [26] J. Y. Shi, S. M. Yiu, Y. Li, H. C. Leung, F. Y. Chin, Predicting drug-target interaction for new drugs using enhanced similarity measures and super-target

- p>clustering,
- Methods*
- 83 (2015) 98–104. doi:10.1016/j.ymeth.2015.04.036.
- 
- URL
- <http://dx.doi.org/10.1016/j.ymeth.2015.04.036>
- [27] N. J. Perualila-Tan, Z. Shkedy, W. Talloen, H. W. Göhlmann, M. V. Van Moerbeke, A. Kasim, Weighted similarity-based clustering of chemical structures and bioactivity data in early drug discovery, *Journal of Bioinformatics and Computational Biology* doi:10.1142/S0219720016500189.
- [28] T. Pahikkala, A. Airola, S. Pietilä, S. Shakyawar, A. Szwajda, J. Tang, T. Aittokallio, Toward more realistic drug-target interaction predictions, *Briefings in Bioinformatics* 16 (2) (2015) 325–337. doi:10.1093/bib/bbu010.
- [29] K. Sachdev, M. K. Gupta, A comprehensive review of feature based methods for drug target interaction prediction (2019). doi:10.1016/j.jbi.2019.103159.
- [30] Z. Liu, F. Guo, J. Gu, Y. Wang, Y. Li, D. Wang, L. Lu, D. Li, F. He, Similarity-based prediction for Anatomical Therapeutic Chemical classification of drugs by integrating multiple data sources, in: *Bioinformatics*, 2015. doi:10.1093/bioinformatics/btv055.
- [31] T. He, M. Heidemeyer, F. Ban, A. Cherkasov, M. Ester, SimBoost: a read-across approach for predicting drug-target binding affinities using gradient boosting machines, *Journal of Cheminformatics* 9 (1) (2017) 1–14. doi:10.1186/s13321-017-0209-z.
- [32] K. Xu, J. Ba, R. Kiros, K. Cho, A. Courville, R. Salakhudinov, R. Zemel, Y. Bengio, Show, attend and tell: Neural image caption generation with visual attention, in: F. Bach, D. Blei (Eds.), *Proceedings of the 32nd International Conference on Machine Learning*, Vol. 37 of *Proceedings of Machine Learning Research*, PMLR, Lille, France, 2015, pp. 2048–2057.  
URL <http://proceedings.mlr.press/v37/xuc15.html>
- [33] D. Bahdanau, K. Cho, Y. Bengio, Neural Machine Translation by Jointly Learning to Align and Translate (2014) 1–15 [arXiv:1409.0473](https://arxiv.org/abs/1409.0473).  
URL <http://arxiv.org/abs/1409.0473>
- [34] I. Wallach, M. Dzamba, A. Heifets, AtomNet: A Deep Convolutional Neural Network for Bioactivity Prediction in Structure-based Drug Discovery (2015) 1–

11arXiv:1510.02855, doi:10.1007/s10618-010-0175-9.

URL <http://arxiv.org/abs/1510.02855>

- [35] S. Kearnes, K. McCloskey, M. Berndl, V. Pande, P. Riley, Molecular graph convolutions: moving beyond fingerprints, *Journal of Computer-Aided Molecular Design* 30 (8) (2016) 595–608. doi:10.1007/s10822-016-9938-8.
- [36] J. Gomes, B. Ramsundar, E. N. Feinberg, V. S. Pande, Atomic Convolutional Networks for Predicting Protein-Ligand Binding Affinity, *arXiv e-prints* (2017) 1–17arXiv:1703.10603, doi:10.18653/v1/P16-1228.  
URL <http://arxiv.org/abs/1703.10603>
- [37] H. Altae-Tran, B. Ramsundar, A. S. Pappu, V. Pande, Low Data Drug Discovery with One-Shot Learning, *ACS Central Science*arXiv:1611.03199, doi:10.1021/acscentsci.6b00367.
- [38] D. Weininger, SMILES, a Chemical Language and Information System: 1: Introduction to Methodology and Encoding Rules, *Journal of Chemical Information and Computer Sciences*doi:10.1021/ci00057a005.
- [39] G. Landrum, RDKit: Open-source Cheminformatics (2006). doi:10.2307/3592822.
- [40] D. S. Cao, Q. S. Xu, Y. Z. Liang, Propy: A tool to generate various modes of Chou’s PseAAC, *Bioinformatics* 29 (7) (2013) 960–962. doi:10.1093/bioinformatics/btt072.
- [41] R. Todeschini, V. Consonni, *Molecular Descriptors for Chemoinformatics*, Wiley, 2010. doi:10.1002/9783527628766.
- [42] S. M. Mahmud, W. Chen, H. Meng, H. Jahan, Y. Liu, S. M. Hasan, Prediction of drug-target interaction based on protein features using undersampling and feature selection techniques with boosting, *Analytical Biochemistry* 589 (November 2019) (2020) 113507. doi:10.1016/j.ab.2019.113507.  
URL <https://doi.org/10.1016/j.ab.2019.113507>
- [43] A. Cereto-Massagu, M. J. Ojeda, C. Valls, M. Mulero, S. Garcia-Vall, G. Pujadas, Molecular fingerprint similarity search in virtual

- screening, *Methods* 71 (2015) 58 – 63, virtual Screening. doi:<https://doi.org/10.1016/j.ymeth.2014.08.005>.  
URL <http://www.sciencedirect.com/science/article/pii/S1046202314002631>
- [44] T. Kogej, O. Engkvist, N. Blomberg, S. Muresan, Multifingerprint based similarity searches for targeted class compound selection, *Journal of Chemical Information and Modeling* doi:10.1021/ci0504723.
- [45] J. Duan, S. L. Dixon, J. F. Lowrie, W. Sherman, Analysis and comparison of 2d fingerprints: Insights into database screening performance using eight fingerprint methods, *Journal of Molecular Graphics and Modelling* 29 (2) (2010) 157 – 170. doi:<https://doi.org/10.1016/j.jmgm.2010.05.008>.  
URL <http://www.sciencedirect.com/science/article/pii/S1093326310000781>
- [46] R. Sawada, M. Kotera, Y. Yamanishi, Benchmarking a wide range of chemical descriptors for drug-target interaction prediction using a chemogenomic approach (2014). doi:10.1002/minf.201400066.
- [47] O. Soufan, W. Ba-Alawi, M. Afeef, M. Essack, P. Kalnis, V. B. Bajic, DRABAL: novel method to mine large high-throughput screening assays using Bayesian active learning, *Journal of Cheminformatics* doi:10.1186/s13321-016-0177-8.
- [48] T. Baltrusaitis, C. Ahuja, L. P. Morency, Multimodal Machine Learning: A Survey and Taxonomy, *IEEE Transactions on Pattern Analysis and Machine Intelligence* 41 (2) (2019) 423–443. arXiv:1705.09406v2, doi:10.1109/TPAMI.2018.2798607.
- [49] D. Duvenaud, D. Maclaurin, J. Aguilera-Iparraguirre, R. Gómez-Bombarelli, T. Hirzel, A. Aspuru-Guzik, R. P. Adams, Convolutional Networks on Graphs for Learning Molecular Fingerprints (2015) 1–9 arXiv:1509.09292.  
URL <http://arxiv.org/abs/1509.09292>
- [50] Z. Wu, B. Ramsundar, E. N. Feinberg, J. Gomes, C. Geniesse, A. S. Pappu, K. Leswing, V. Pande, MoleculeNet: A benchmark for molecular machine learning, *Chemical Science* 9 (2) (2018) 513–530. arXiv:1703.00564, doi:10.1039/c7sc02664a.

- [51] M. Tsubaki, K. Tomii, J. Sese, Compound-protein interaction prediction with end-to-end learning of neural networks for graphs and sequences, *Bioinformatics* 35 (2) (2019) 309–318. doi:10.1093/bioinformatics/bty535.
- [52] Q. Feng, E. Dueva, A. Cherkasov, M. Ester, PADME: A Deep Learning-based Framework for Drug-Target Interaction Prediction (2018) 1–21arXiv:1807.09741.  
URL <http://arxiv.org/abs/1807.09741>
- [53] B. Agyemang, W. Wu, M. Y. Kpiebaareh, E. Nanor, Drug-target indication prediction by integrating end-to-end learning and fingerprints, in: 2019 16th International Computer Conference on Wavelet Active Media Technology and Information Processing, 2019, pp. 266–272. doi:10.1109/ICCWAMTIP47768.2019.9067510.  
URL <https://ieeexplore.ieee.org/document/9067510>
- [54] D. Rogers, M. Hahn, Extended-Connectivity Fingerprints, *Journal of Chemical Information and Modeling* 50 (5) (2010) 742–754. doi:10.1021/ci100050t.  
URL <https://doi.org/10.1021/ci100050t>
- [55] T. Pahikkala, A. Airola, S. Pietilä, S. Shakyawar, A. Szwajda, J. Tang, T. Aittokallio, Toward more realistic drug-target interaction predictions, *Briefings in Bioinformatics*doi:10.1093/bib/bbu010.
- [56] H. Öztürk, A. Özgür, E. Ozkirimli, DeepDTA: Deep drug-target binding affinity prediction, *Bioinformatics* 34 (17) (2018) i821–i829. arXiv:1801.10193, doi:10.1093/bioinformatics/bty593.
- [57] J. T. Metz, E. F. Johnson, N. B. Soni, P. J. Merta, L. Kifle, P. J. Hajduk, Navigating the kinome, *Nature Chemical Biology*doi:10.1038/nchembio.530.
- [58] K. Pliakos, C. Vens, G. Tsoumakas, Predicting drug-target interactions with multi-label classification and label partitioning, *IEEE/ACM Transactions on Computational Biology and Bioinformatics PP (JANUARY)* (2019) 1–1. doi:10.1109/TCBB.2019.2951378.  
URL <https://ieeexplore.ieee.org/document/8890853/>



- [59] Y. Tabei, E. Pauwels, V. Stoven, K. Takemoto, Y. Yamanishi, Identification of chemogenomic features from drug-target interaction networks using interpretable classifiers, *Bioinformatics* 28 (18) (2012) 487–494. doi:10.1093/bioinformatics/bts412.
- [60] C. dos Santos, M. Tan, B. Xiang, B. Zhou, Attentive Pooling Networks (Cv). *arXiv:1602.03609*.  
URL <http://arxiv.org/abs/1602.03609>
- [61] A. Vaswani, G. Brain, N. Shazeer, N. Parmar, J. Uszkoreit, L. Jones, A. N. Gomez, L. Kaiser, I. Polosukhin, Attention Is All You Need, *Advances in neural information processing systems (Nips)* (2017) 5998–6008.  
URL <http://papers.nips.cc/paper/7181-attention-is-all-you-need.pdf>
- [62] K. Yingkai Gao, A. Fokoue, H. Luo, A. Iyengar, S. Dey, P. Zhang, Interpretable drug target prediction using deep neural representation, *IJCAI International Joint Conference on Artificial Intelligence 2018-July* (2018) 3371–3377.
- [63] Y. Yamanishi, M. Kotera, M. Kanehisa, S. Goto, Drug-target interaction prediction from chemical, genomic and pharmacological data in an integrated framework, *Bioinformatics*doi:10.1093/bioinformatics/btq176.
- [64] Y. Luo, X. Zhao, J. Zhou, J. Yang, Y. Zhang, W. Kuang, J. Peng, L. Chen, J. Zeng, A network integration approach for drug-target interaction prediction and computational drug repositioning from heterogeneous information, *Nature Communications* 8 (1). doi:10.1038/s41467-017-00680-8.  
URL <http://dx.doi.org/10.1038/s41467-017-00680-8>
- [65] Y. Wang, H. Chang, J. Wang, Y. Shi, Drug-target interaction prediction based on heterogeneous networks, *ACM International Conference Proceeding Series Part F1432* (2018) 14–18. doi:10.1145/3278198.3278204.
- [66] S. Cao, W. Lu, Q. Xu, GraRep: Learning graph representations with global structural information, in: *International Conference on Information and Knowledge Management, Proceedings*, 2015. doi:10.1145/2806416.2806512.
- [67] Y. Liu, M. Wu, C. Miao, P. Zhao, X. L. Li, Neighborhood Regularized Logistic

Matrix Factorization for Drug-Target Interaction Prediction, PLoS Computational Biology doi:10.1371/journal.pcbi.1004760.

- [68] H. E. Manoochehri, M. Nourani, Predicting Drug-Target Interaction Using Deep Matrix Factorization, 2018 IEEE Biomedical Circuits and Systems Conference, BioCAS 2018 - Proceedings (2018) 1–4 doi:10.1109/BIOCAS.2018.8584817.
- [69] N. Yasuo, Y. Nakashima, M. Sekijima, CoDe-DTI: Collaborative Deep Learning-based Drug-Target Interaction Prediction, Proceedings - 2018 IEEE International Conference on Bioinformatics and Biomedicine, BIBM 2018 (2018) 792–797 doi:10.1109/BIBM.2018.8621368.
- [70] S. M. Nair, J. George, A Novel Method For Drug Target Interaction Prediction, International Journal of Computer Engineering & Technology (IJCET 9 (3) (2018) 105–114.  
 URL <http://www.iaeme.com/IJCET/index.asp105http://www.iaeme.com/ijcet/issues.asp?JType=IJCT{&}VType=9{&}IType=3JournalImpactFactor{&}0Awww.jifactor.comhttp://www.iaeme.com/IJCET/index.asp106http://www.iaeme.com/ijcet/issues.asp?JType=IJCT{&}VType=9{&}IType=3>
- [71] L. Jacob, J. P. Vert, Protein-ligand interaction prediction: An improved chemogenomics approach, Bioinformatics doi:10.1093/bioinformatics/btn409.
- [72] K. Bleakley, Y. Yamanishi, Supervised prediction of drug-target interactions using bipartite local models, Bioinformatics doi:10.1093/bioinformatics/btp433.
- [73] H. Öztürk, E. Ozkirimli, A. Özgür, A comparative study of SMILES-based compound similarity functions for drug-target interaction prediction, BMC Bioinformatics doi:10.1186/s12859-016-0977-x.
- [74] H. Ding, I. Takigawa, H. Mamitsuka, S. Zhu, Similarity-based machine learning methods for predicting drug-target interactions: A brief review, Briefings in Bioinformatics 15 (5) (2013) 734–747. doi:10.1093/bib/bbt056.
- [75] F. Rayhan, S. Ahmed, D. Md Farid, A. Dehzangi, S. Shatabda, CFSBoost: Cumulative feature subspace boosting for drug-target interaction prediction, Journal of Theoretical Biology doi:10.1016/j.jtbi.2018.12.024.

- [76] C. Orellana M, R. Nănculef, C. Valle, Boosting collaborative filters for drug-target interaction prediction, in: Lecture Notes in Computer Science (including subseries Lecture Notes in Artificial Intelligence and Lecture Notes in Bioinformatics), 2018. doi:10.1007/978-3-030-13469-3\_25.
- [77] A. Niculescu-Mizil, R. Caruana, Obtaining calibrated probabilities from boosting, Proceedings of the 21st Conference on Uncertainty in Artificial Intelligence, UAI 2005 (2005) 413–420arXiv:1207.1403.
- [78] K. Yang, Z. Zhang, S. He, X. Bo, Prediction of DTIs for high-dimensional and class-imbalanced data based on CGAN, Proceedings - 2018 IEEE International Conference on Bioinformatics and Biomedicine, BIBM 2018 (2018) 788–791doi: 10.1109/BIBM.2018.8621098.
- [79] T. Mikolov, K. Chen, G. Corrado, J. Dean, Efficient estimation of word representations in vector space, 1st International Conference on Learning Representations, ICLR 2013 - Workshop Track Proceedings (2013) 1–12arXiv:1301.3781.
- [80] J. Pennington, R. Socher, C. D. Manning, GloVe: Global vectors for word representation, in: EMNLP 2014 - 2014 Conference on Empirical Methods in Natural Language Processing, Proceedings of the Conference, 2014. doi: 10.3115/v1/d14-1162.
- [81] E. Asgari, M. R. Mofrad, Continuous distributed representation of biological sequences for deep proteomics and genomics, PLoS ONE 10 (11) (2015) 1–15. doi:10.1371/journal.pone.0141287.
- [82] D. S. Wishart, Y. D. Feunang, A. C. Guo, E. J. Lo, A. Marcu, J. R. Grant, T. Sajed, D. Johnson, C. Li, Z. Sayeeda, N. Assempour, I. Iynkkaran, Y. Liu, A. MacIejewski, N. Gale, A. Wilson, L. Chin, R. Cummings, D. Le, A. Pon, C. Knox, M. Wilson, DrugBank 5.0: A major update to the DrugBank database for 2018, Nucleic Acids Researchdoi:10.1093/nar/gkx1037.
- [83] S. Dallakyan, A. J. Olson, Small-Molecule Library Screening by Docking with PyRx, Springer New York, New York, NY, 2015, pp. 243–250. doi:10.1007/978-1-4939-2269-7\_19.  
URL [https://doi.org/10.1007/978-1-4939-2269-7\\_19](https://doi.org/10.1007/978-1-4939-2269-7_19)

- [84] N. Blom, S. Gammeltoft, S. Brunak, Sequence and structure-based prediction of eukaryotic protein phosphorylation sites, *Journal of Molecular Biology* doi: 10.1006/jmbi.1999.3310.